Astronomy & Astrophysics

On the origin of [NeII] 12.81 μm emission from pre-main sequence stars: Disks, jets, and accretion⋆

M. Güdel[1,2,3,4], F. Lahuis[5,4], K. R. Briggs[2], J. Carr[6], A. E. Glassgold[7], Th. Henning[3], J. R. Najita[8], R. van Boekel[3], and E. F. van Dishoeck[4,9]

[1] University of Vienna, Department of Astronomy, Türkenschanzstrasse 17, 1180 Vienna, Austria
e-mail: manuel.guedel@univie.ac.at
[2] ETH Zurich, Institute of Astronomy, 8093 Zurich, Switzerland
[3] Max-Planck-Institute for Astronomy, Königstuhl 17, 69117 Heidelberg, Germany
[4] Leiden Observatory, Leiden University, PO Box 9513, 2300 RA Leiden, The Netherlands
[5] SRON Netherlands Institute for Space Research, PO Box 800, 9700 AV Groningen, The Netherlands
[6] Naval Research Laboratory, Code 7213, Washington, DC 20375, USA
[7] University of California at Berkeley, Berkeley, CA 94720, USA
[8] National Optical Astronomy Observatory, 950 N. Cherry Ave., Tucson, AZ 85719, USA
[9] Max-Planck Institut für Extraterrestrische Physik (MPE), Giessenbachstr. 1, 85748 Garching, Germany

ABSTRACT

Context. Extreme-ultraviolet (EUV) and X-ray photons from classical T Tauri stars are powerful ionization and heating agents that drive disk chemistry, disk instabilities, and photoevaporative flows. The mid-infrared fine-structure line of [Ne II] at 12.81 μm has been proposed to trace gas in disk surface layers heated and ionized by stellar X-ray and EUV radiation.
Aims. We aim at locating the origin of [Ne II] line emission in circumstellar environments by studying distributions of [Ne II] emission and correlating the inferred [Ne II] luminosities, $L_{[\text{Ne II}]}$, with stellar and circumstellar disk parameters.
Methods. We have conducted a study of [Ne II] line emission based on a sample of 92 pre-main sequence stars mostly belonging to the infrared Class II, but including 13 accreting transition disk objects, and also 14 objects that drive known jets and outflows.
Results. We find several significant correlations between $L_{[\text{Ne II}]}$ and stellar parameters, in particular L_X and the wind mass loss rate, $\dot{M}_{\text{loss}}$. Most correlations are, however, strongly dominated by systematic scatter of unknown origin. While there is a positive correlation between $L_{[\text{Ne II}]}$ and L_X, the stellar mass accretion rate, $\dot{M}_{\text{acc}}$, induces a correlation only if we combine the largely different subsets of jet sources and stars without jets. Our results indeed suggest that $L_{[\text{Ne II}]}$ is bi-modally distributed, with separate distributions for the two subsamples. The jet sources show systematically higher $L_{[\text{Ne II}]}$, by 1–2 orders of magnitude with respect to objects without jets. Jet-driving stars also tend to show higher mass accretion rates. We therefore hypothesize that the trend with $\dot{M}_{\text{acc}}$ only reflects a trend with $\dot{M}_{\text{loss}}$ that is more physically relevant for [Ne II] emission.
Conclusions. The [Ne II] luminosities measured for objects without known outflows and jets are found to agree with simplified calculations of [Ne II] emission from disk surface layers if the measured stellar X-rays are responsible for heating and ionizing the gas. The large scatter in $L_{[\text{Ne II}]}$ may be introduced by variations of disk properties and the irradiation spectrum, as previously suggested. If these additional factors can be sufficiently well constrained, then the [Ne II] 12.81 μm line should be an important diagnostic for disk surface ionization and heating, at least in the inner disk region. This applies in particular to transition disks also included in our sample. The systematically enhanced [Ne II] flux from jet sources clearly suggests a role for the jets themselves, as previously demonstrated by a spatially resolved observation of the outflow system in the T Tau triple.

Key words. stars: formation – stars: pre-main sequence – protoplanetary disks

1. Introduction

Circumstellar dust disks are the most important element in the process of planet formation. They have been well studied in resolved images, through the mid-infrared 10 μm silicate feature, and through continuum emission all the way from the near-infrared to the millimeter domain. Such studies have demonstrated ongoing grain growth and settling of dust to the disk midplane (e.g., van Boekel et al. 2003) as well as the presence of inner dust-disk holes (e.g., Bouwman et al. 2003).

However, dust contributes only about 1% to the total disk mass. The gas in which the dust is immersed is much more

challenging to observe; yet, gas is fundamentally important to determine temperature and density gradients in the disk, to drive a chemistry forming important molecules, and to control the dynamics of the dust itself. Growing, massive, gas-rich planets will accrete their extended atmospheres from this gas reservoir. Knowing the gas content and the conditions of the gas phase is therefore fundamental to develop models of planet formation, a deeper understanding of the early evolution of planetary atmospheres, and eventually of the chemistry on planets. However, gas disks are difficult to observe because high spatial resolution spectroscopy in the mm and sub-mm range is still challenging, and optically thin molecular lines in the mid-infrared are often faint; promising, pioneering studies have been performed (Dutrey et al. 1997; Simon et al. 2000; Lahuis et al. 2006, 2007; Bitner et al. 2007), including observations of CO and H_2 in the

---

⋆ Complete Tables 1–4 are only available in electronic form at http://www.aanda.org

inner, "terrestrial" planet-forming disk region (Herczeg et al. 2002; Najita et al. 2003; Blake & Boogert 2004) and also detections of organic molecules and water at larger radii (Lahuis et al. 2006; Carr & Najita 2008; Salyk et al. 2008).

Recent studies, both theoretical (Glassgold et al. 2004; Jonkheid et al. 2004; Kamp & Dullemond 2004; Nomura & Millar 2005; Glassgold et al. 2007) and observational (Weintraub et al. 2000; Herczeg et al. 2002) have suggested that short-wavelength radiation (ultraviolet [UV], extreme ultraviolet [EUV], and X-rays) from the central star significantly affects circumstellar disks in several ways. High-energy photons are capable of ionizing the upper layer of circumstellar disks at a level orders of magnitude in excess of what cosmic rays could achieve (Igea & Glassgold 1999; Glassgold et al. 2004; Ilgner & Nelson 2006). Even weak ionization of the surface layer will, in combination with magnetic fields, induce the magnetorotational instability (Balbus & Hawley 1991), leading to accretion from the surface layer while the deeper zones of the disk may remain shielded and thus provide ideal environments for planet formation.

Detection of the environmental impact of X-rays and EUV photons is, however, challenging. Some direct evidence for the relevant processes is provided by X-rays themselves; fluorescence of cold iron as seen in the X-ray range at 6.4 keV has been interpreted as being due to irradiation of the disk surface by hard X-ray photons from the stellar magnetosphere (Imanishi et al. 2001; Tsujimoto et al. 2005; Favata et al. 2005). Photoelectric absorption of stellar X-rays by disk material can be directly measured in particular in cases for which the disk is seen at high inclination angles (Kastner et al. 2005).

The same interactions also heat the disk surface layers to several thousand K, generating a "disk chromosphere" that decouples from the dust component. Strong UV continuum and fluorescence (Bergin et al. 2004; Herczeg et al. 2002, 2006) and pure rotational and rovibrational IR transitions of H_2 (Weintraub et al. 2000; Bary et al. 2003; Bitner et al. 2007) require high ($\sim$1000 K) disk gas temperatures. This warm disk gas may also have been detected through CO emission (Najita et al. 2003; Blake & Boogert 2004; Brittain et al. 2007) and in fine-structure transitions of [Ne II] after ionization by EUV/X-ray photons, as further discussed below. As a most important by-product of ionization and heating, chemistry is driven across temperature gradients in the disks, especially in UV shielded regions (Aikawa & Herbst 1999). Furthermore, disk photoevaporation due to X-ray or EUV heating of the inner disk has attracted increasing attention (Alexander et al. 2004; Ercolano et al. 2008; Gorti et al. 2009).

Short-wavelength disk irradiation is thus of central interest for our understanding of the ionization of circumstellar disks, their heating and chemical processing, disk instabilities, and photoevaporation and therefore the long-term evolution of disks. All these mechanisms obviously affect the process of planet formation.

2. The Ne II 12.81 μm diagnostic

Glassgold et al. (2007) proposed that the mid-infrared [Ne II] fine-structure transition at 12.81 μm is a tracer of *warm* gas requiring X-ray irradiation of the disk. Because the first ionization potential of Ne is high (21.6 eV), its photoionization indeed requires EUV or X-ray photons. In the X-ray ionization model of Glassgold et al. (2007) Ne is ionized by K-shell absorption, requiring photons with energies of at least 0.9 keV. As

the same X-rays also heat the upper layers of the gas disk to several 1000 K (Glassgold et al. 2004), [Ne II] fine-structure transitions with excitation temperatures of $\approx$1000 K are produced over a scale height of warm gas of 10^{19}–10^{20} cm^{-2}. An alternative model (Hollenbach & Gorti 2009; see also Gorti & Hollenbach 2008) proposes ionization of the disk surface by EUV radiation, producing an H II-like highly-ionized region in which the [Ne II] line is formed. The [Ne II] transition thus appears to be an ideal tracer both of disk gas and of the environmental impact of high-energy stellar radiation.

[Ne II] emissivities were also calculated for shocks in molecular clouds, e.g. such as those forming when a protostellar jet rams into the surrounding molecular gas (e.g., Hollenbach & McKee 1989). The Infrared Space Observatory (ISO) indeed detected the [Ne II] line feature in the T Tau system (van den Ancker et al. 1999); the authors attributed this line to shocks in the outflows of the T Tau system. The [Ne II] line has also been seen in Herbig-Haro objects (Neufeld et al. 2006).

The advent of the *Spitzer Space Telescope* (*Spitzer* henceforth; Werner et al. 2004) has renewed interest in the [Ne II] feature from pre-main sequence stars as theoretical calculations of X-ray irradiated circumstellar disks (Glassgold et al. 2007) predicted easy detection by the Infrared Spectrometer (IRS; Houck et al. 2004). Follow-up calculations have confirmed and deepened these initial predictions (Meijerink et al. 2008), also including EUV irradiation (Hollenbach & Gorti 2009). First successful detections of the [Ne II] line by the IRS were reported by Pascucci et al. (2007), Espaillat et al. (2007), Lahuis et al. (2007), and Ratzka et al. (2007) from a variety of pre-main sequence objects with circumstellar disks and partly also with protostellar envelopes. Initial attempts were made to relate the observed [Ne II] fluxes to stellar or disk properties, but the mostly small samples yielded ambiguous results. Pascucci et al. (2007) claimed a correlation between the luminosity in the [Ne II] line, $L_{\text{[Ne II]}}$, and the stellar X-ray luminosity, L_X, but the sample contained only four detections distributed in L_X over a mere 0.2 dex, which corresponds to the usual range of variability of stellar coronal X-ray emission. A correlation with the stellar mass accretion rate, $\dot{M}_{\text{acc}}$, was not found. Conversely, Espaillat et al. (2007) suggested $L_{\text{[Ne II]}}$ to be correlated with $\dot{M}_{\text{acc}}$ but not with L_X, but again, the data sample and the dynamic range in L_X were small ($\approx$0.8 dex). Finally, Lahuis et al. (2007) considered [Ne II] line production both as a consequence of X-ray or EUV irradiation of disks and of shock formation on the disks themselves. They noticed that the measured $L_{\text{[Ne II]}}$ correspond well to predictions made by Glassgold et al. (2007).

Ground-based observations of the [Ne II] line allow for much higher spectral resolving power, uncovering the kinematics of the emitting regions. Herczeg et al. (2007) observed a relatively narrow profile in the near-pole-on system TW Hya, interpreting the emission as coming either from the disk surface (i.e., from a region where the gas is gravitationally bound), or a slow photoevaporative flow from a disk region that allows for escaping gas flows given a sufficiently high gas temperature. [Ne II] emission from such flows was indeed modeled by Alexander (2008), their results being consistent with the observations. Additional support came from high spectral resolution observations of transition disks; three objects of this class showed line profiles and blue-shifts consistent with those predicted from photoevaporative flows (Pascucci & Sterzik 2009). Further ground-based observations of AA Tau and GM Aur with the TEXES instrument clearly show that most of their [Ne II] emission is consistent with a disk origin although the lower fluxes, when compared with *Spitzer* results, suggest that there is also an extended component

(not recovered by the narrow slit of TEXES). Alternatively, the sources may be time-variable, or the line is spectrally unusually broad (Najita et al. 2009).

A rather unexpected twist came with the observation of the T Tauri system with the VLT at high spectral resolution (van Boekel et al. 2009). Here, the [Ne II] emission region was clearly extended (by several arcseconds) and showed line broadening and line shifts (by up to 126 km s^{-1}) compatible with the jets of the T Tauri system, previously observed in a similar fashion in [S II] and [O I] by Böhm & Solf (1994). The interpretation favored shock-induced [Ne II] formation, but X-ray irradiation by the star and consequent ionization of the jet material remains a viable option (van Boekel et al. 2009). This scenario (stellar X-rays ionizing the jet, and [Ne II] emission forming in the jet itself) has recently been suggested on theoretical grounds as well (Shang et al. 2010).

The variety of possible formation scenarios of the [Ne II] line and the large range of stellar and disk properties, including the presence of jets and outflows in some of the systems, calls for a deeper investigation requiring a much larger sample. To this end, we have started a comprehensive study of [Ne II] emission from classical T Tauri stars (CTTS) in particular in the context of X-ray emission and measured mass accretion rates. Our goal has been to revisit recent work that was based mostly on small samples or observations of individual objects, and to analyze and study the combined sample of objects in a systematic way. We have re-analyzed many of the previously reported [Ne II] data (mostly from *Spitzer*) coherently, but we have also added crucial new observations from our dedicated observing programs. The present work also for the first time presents a uniform, archival study of all available X-ray data from the *XMM-Newton* and *Chandra* observatories for these sources, complemented with data from new observing programs. The increased sensitivity and spectral resolving power of these X-ray devices permit a much better characterization of the stellar X-ray radiation than hitherto possible with data from, e.g., ROSAT as used in earlier [Ne II] studies (Lahuis et al. 2007; Pascucci et al. 2007). We will further use ancillary data collected from the published literature, such as mass accretion rates or mass outflow rates. We also refer to forthcoming work by Baldovin-Saavedra et al. (2010) in which a sample of gas lines (of H$_2$, [Ne II], [Ne III], [Fe II], [S III]) in the IRS spectal range is discussed but for a more confined sample of pre-main sequence stars in Taurus; few significant correlations are reported there, the most likely one again supporting an origin of [Ne II] emission in outflows.

Initial results of our work are described in Güdel et al. (2009a). In short, indications of a correlation of $L_{\rm [Ne II]}$ with both $L_{\rm X}$ and $\dot{M}_{\rm acc}$ were found, but strong scatter dominates these correlations. However, it was also found that *sources with jets* show consistently higher $L_{\rm [Ne II]}$, and that $L_{\rm [Ne II]}$ seems to correlate with wind or outflow properties. The purpose of the present paper is to present our entire data set and additional correlation studies, and to coherently discuss these results.

3. Stellar sample

Given the presently favored models for [Ne II] line emission, we selected targets for our study that have well-observed disks and may also be engines of jets an outflows, but we did not include Class I objects in which a number of additional circumstellar regions may be relevant for [Ne II] emission, such as shocks on disks produced by material accreting from the envelope, the irradiated envelopes themselves, shocks between the jets or outflows and the envelopes, etc. Further, strong extinction

and photoelectric absorption make Class I objects difficult for study. Sufficiently strong extinction may suppress some infrared emission from the regions close to the star selectively. Also, only a moderate fraction of Class I sources is accessible by modern X-ray satellites, and the detected X-ray emission is, due to photoelectric absorption, relatively hard (photon energies typically >2 keV). The bulk part of the X-ray emission therefore remains undetected, and an unbiased reconstruction of the underlying (intrinsic) X-ray emission relies on assumptions. For a study predominantly based on [Ne II] detections of Class I sources, see Flaccomio et al. (2009).

Our targets were therefore required to be essentially Class II objects or (accreting) CTTS. More massive Herbig stars were not considered given their considerable UV radiation fields and possibly very different X-ray source properties (Telleschi et al. 2007a). On the other hand, CTTS ejecting jets were intentionally included because jets may play a crucial role in strongly accreting CTTS, and they may be directly linked to the accretion process itself. Including such objects will therefore allow us to investigate to what extent jets matter for the observed [Ne II] emission, and perhaps to identify a subset of objects showing a baseline [Ne II] flux unaffected by jets. To study this latter possibility further, a few targets revealing signatures of transition disks, i.e., disks with inner holes, have been included. Transition disks may also be important to discriminate between X-ray and EUV-related [Ne II] emission models as the potentially low gas content in the inner disk may make this region transparent to direct EUV radiation (see, e.g., numerical models by Alexander et al. 2006).

The data selection is primarily driven by the availability of [Ne II] observations (detections or upper limits). Our sample is therefore mostly drawn from observations available in the *Spitzer* IRS data archive. The largest part of our target list originates from the Lahuis et al. (2007) survey (based on the *Spitzer Cores to Disk [c2d]* legacy program; Evans et al. 2003). This survey focuses on the NGC 1333, Chamaeleon, Lupus, Rho Oph, and Serpens star forming regions, all with characteristic ages of a few Myr. Compared to the preliminary presentation in Güdel et al. (2009a), we have reduced these data again using a new, improved software version with more careful background subtraction and treatment of potential blends, resulting in many additional detections not used in the initial report.

To this sample, we added several targets from our *Spitzer general observer* programs (PI J. Carr). This sample in particular includes objects from the Taurus star forming region, and some targets from Chamaeleon and Rho Oph. Further [Ne II] fluxes or upper limits thereof were adopted from the published literature, in particular for RX J1111.7-7620, PZ99 J161411, RX J1842.9-3542, and RX J1852.3-3700 (Pascucci et al. 2007), observed as part of the *Spitzer Formation and Evolution of Planetary Systems (FEPS)* legacy program (Meyer et al. 2004), DP Tau observed with the *MICHELLE* spectrograph at Gemini North (Herczeg et al. 2007), and T Tau N and S observed with the *VISIR* spectrograph at the Very Large Telescope (VLT) (van Boekel et al. 2009). These references describe the respective data reduction in detail.

Our targets and their properties are listed in Tables 1–4 (the first ten entries are displayed; the complete tables are available in the electronic version of this paper). Table 1 lists the adopted stellar names, the same as those used in the original literature reporting portions of our [Ne II] sample; some common alternative names are also given. The table further gives J2000.0 coordinates and adopted distances; all entries are ordered in increasing RA. The targets are arranged identically in the subsequent

Table 1. Targets (first ten entries).

Star	Alternative names	RA(J2000.0) (h m s)	Dec(J2000.0) (deg ′ ″)	dist. (pc)
RNO 15	HBC 339, CoKu NGC 1333/2	03 27 47.7	30 12 04.3	250
LkHα 270	HBC 12, NGC 1333 IRS 2	03 29 17.7	31 22 45.1	250
LkHα 271	HBC 13	03 29 21.9	31 15 36.4	250
LkHα 326	HBC 14	03 30 44.0	30 32 46.7	250
LkHα 327	HBC 15, IRAS 03304+3100	03 33 30.4	31 10 50.5	250
LkHα 330	HBC 20, IRAS F03426+3214	03 45 48.3	32 24 11.9	250
IRAS 03446+3254	IRS 4	03 47 47.1	33 04 03.4	250
BP Tau	HBC 32, HD 281934, IRAS 04161+2859	04 19 15.8	29 06 26.9	140
FM Tau	HBC 23, Haro 6-1	04 14 13.6	28 12 49.2	140
T Tau N	HBC 35, HD 284419, IRAS 04190+1924	04 21 59.4	19 32 06.4	140

Table 2. Mid-IR and X-ray observations (first ten entries).

Star	*Spitzer* AOR[a]	X-ray ObsID[b]	X-ray start time[c] y-m-d h:m:s	X-ray stop time[c] y-m-d h:m:s	Total X-ray exposure[c] (s)
RNO 15	5633280	0503670101	2007-07-31 04:55:25	2007-07-31 15:32:31	33 135
LkHα 270	5634048	0065820101	2002-02-27 22:48:25	2002-02-28 12:41:45	44 808
LkHα 271	11827968	0065820101	2002-02-27 22:48:25	2002-02-28 12:41:45	44 808
LkHα 326	5634304	...	...	...	...
LkHα 327	5634560	...	...	...	...
LkHα 330	5634816	...	...	...	...
IRAS 03446+3254	5635072	...	...	...	...
BP Tau	14548224	0200370101	2004-08-15 06:36:51	2004-08-16 18:42:57	116 334
FM Tau	15119872	0203542001	2004-09-12 07:21:01	2004-09-12 15:47:38	26 760
T Tau N	(VLT)	0301500101	2005-08-15 14:14:33	2005-08-16 12:55:22	65 810

Notes. [a] *Spitzer* AOR = Astronomical Observation Request; for further details on observing setup, see references in Table 3. [b] *XMM-Newton* observation identification number if not otherwise noted; *Chandra* ID if "(CXO)" added. [c] Exposure start and stop times for the *XMM-Newton* EPIC pn camera if not otherwise noted; if (M1), (M2), (M) added, then MOS1, MOS2, or both MOS were used for analysis, and exposure times refer to those detectors; (+M12) indicates that MOS detectors were used additionally to PN for spectral analysis. Exposure times in last column are livetimes for CCD#1 of *XMM-Newton* camera (CCD containing aimpoint of observation for *Chandra*) and are only detector and are only indicative as intervals with high background were selectively and additionally flagged.

Table 3. Fluxes and luminosities (first ten entries).

Star	$f_{\text{[Ne II]}}$[a] (erg cm^{-2} s^{-1})	$L_{\text{[Ne II]}}$ (erg s^{-1})	$f_{\text{X,0.3-10,abs}}$ (erg cm^{-2} s^{-1})	$L_{\text{X,0.3-10,abs}}$ (erg s^{-1})	$f_{\text{X,0.3-10,unabs}}$ (erg cm^{-2} s^{-1})	$L_{\text{X,0.3-10,unabs}}$ (erg s^{-1})	N_{H}[b] (10^{22})	Refs.[c]
RNO 15	$<2.6(0.85) \times 10^{-14}$	$<1.9 \times 10^{29}$	3.7×10^{-13}	2.8×10^{30}	1.1×10^{-12}	8.0×10^{30}	4.6	1, X
LkHα 270	$1.3(0.35) \times 10^{-14}$	9.7×10^{28}	3.2×10^{-13}	2.4×10^{30}	1.5×10^{-12}	1.1×10^{31}	0.78	1, X
LkHα 271	$<3.6(1.2) \times 10^{-15}$	$<2.7 \times 10^{28}$	3.8×10^{-14}	2.8×10^{29}	1.1×10^{-13}	7.9×10^{29}	3.8	1, X
LkHα 326	$3.1(1.4) \times 10^{-15}$	2.3×10^{28}	...	...	...	...	...	1
LkHα 327	$7.8(3.8) \times 10^{-15}$	5.8×10^{28}	...	...	...	...	...	1
LkHα 330	$3.8(1.9) \times 10^{-15}$	2.8×10^{28}	...	...	...	...	...	1
IRAS 03446+3254	$4.3(0.99) \times 10^{-15}$	3.2×10^{28}	...	...	...	...	...	1, X
BP Tau	$2.9(0.4) \times 10^{-15}$	6.8×10^{27}	4.3×10^{-13}	1.0×10^{30}	6.1×10^{-13}	1.4×10^{30}	0.09	3, X
FM Tau	$<1.1(0.37) \times 10^{-14}$	$<2.6 \times 10^{28}$	1.5×10^{-13}	3.5×10^{29}	2.2×10^{-13}	5.1×10^{29}	0.15	3, X
T Tau N	$2.0(0.4) \times 10^{-13}$	4.7×10^{29}	1.9×10^{-12}	4.4×10^{30}	4.0×10^{-12}	9.4×10^{30}	0.34	5, X

Notes. [a] Errors are given in parentheses. [b] In units of 10^{22} cm^{-2}. [c] Reference: 1: New analysis of Spitzer c2d sample, for original analysis see Lahuis et al. (2007); 2: Pascucci et al. (2007); 3: archival GTO/GO observations, see Najita & Carr (in prep.); 4: Herczeg et al. (2007); 5: van Boekel et al. (2009); 6: Espaillat et al. (2007); C: from *Chandra* archive; X: from *XMM-Newton* archive.

three tables. Table 2 lists observing parameters, namely the Spitzer *Astronomical Observation Request* (AOR; unless observed by another observatory, as indicated), the X-ray observation ID (referring to *XMM-Newton* if not otherwise noted), and the X-ray observation start and stop times together with the total exposure. We note that the full exposure time was not normally used for *XMM-Newton* data analysis as time intervals with high particle background were eliminated to achieve an optimum signal-to-noise ratio (see Güdel et al. 2007a, for details). Table 3 lists our primary results, namely the observed fluxes in the [Ne II] line and the photoelectrically *attenuated* (absorbed, observed) and the modeled *intrinsic*, unabsorbed X-ray fluxes in the 0.3–10 keV range (i.e., the flux measured at Earth if absorption were absent). These fluxes are complemented by the respective luminosities using the distances from Table 1. We also give N_{H} along the line of sight to the star, as derived from

Table 4. Additional parameters (first ten entries).

Star	$\log \dot{M}_{acc}$ ($M_\odot$ yr^{-1})	$EW(H\alpha)$ (Å)	$EW([O I]_f)$ (Å)	$EW([O I]_t)$ (Å)	$\log L_{[OI],f}$ ($L_\odot$)	$\log L_{[OI],t}$ ($L_\odot$)	$\log \dot{M}_{loss}$ ($M_\odot$ yr^{-1})	jet? TD[a]	Refs.[b]
RNO 15	...	...	...	...	...	...	...	...	...
LkHα 270	...	30.9	...	...	...	...	...	...	6
LkHα 271	...	185.7	...	...	...	...	...	...	6
LkHα 326	...	52.7	...	0.8	...	...	...	...	6
LkHα 327	...	51.0	...	0.9	...	...	...	...	6
LkHα 330	...	20.3	...	...	...	...	...	T	6, 31
IRAS 03446+3254	...	...	...	...	...	...	...	...	...
BP Tau	−7.54	40–92	0.07	0.26	−5.71	−4.75	<−9.7	...	13, X, 12
FM Tau	−8.45	62–71	0.045	0.48	−6.37	−5.19	<−10.6	...	21, 35, 6, 12
T Tau N	−7.12	38–60	...	2.0	...	−2.78	−6.96	J	21, 6, 26, 4, (27)

Notes. [a] T = transitional disk (either "anemic" or "cold" disk); J = jet-driving object. [b] References: 1 Alcalá et al. (2008); 2 Bacciotti & Eislöffel (1999); 3 Bally et al. (2006); 4 Böhm & Solf (1994); 5 Briceño et al. (2002); 6 Cohen & Kuhi (1979); 7 Comerón et al. (2003); 8 Espaillat et al. (2007); 9 Gauvin & Strom (1992); 10 Hamann (1994); 11 Hartigan (1993); 12 Hartigan et al. (1995); 13 Hartmann et al. (1998); 14 Herczeg et al. (2004); 15 Herczeg et al. (2005); 16 Herczeg et al. (2007); 17 Hirth et al. (1997); 18 Hughes et al. (1994); 19 Krautter et al. (1997); 20 Luhman (2004); 21 Najita et al. (2007); 22 Pascucci et al. (2007); 23 Rydgren (1980); 24 Seperuelo Duarte et al. (2008); 25 Takami et al. (2003); 26 White & Hillenbrand (2004); 27 Kenyon & Hartmann (1995); 28 Mundt & Eislöffel (1998); 29 Solf & Böhm (1993); 30 Cox et al. (2005); 31 Brown et al. (2007); 32 Calvet et al. (2002); 33 Calvet et al. (2005); 34 Forrest et al. (2004); 35 White & Ghez (2001); 36 Dougados et al. (2000); 37 Hartigan et al. (2004); 38 Najita et al. (2008); 39 Natta et al. (2006); 40 Webb et al. (1999); 41 Alcalá et al. (1993). M: 2MASS; S: SIMBAD; X: XEST survey, see Güdel et al. (2007a) and references therein. References in parentheses are for complementary data, e.g., A_V or R magnitude, used to calculate $\log L_{[OI]}$.

the X-ray spectral fits (see below). All values are given to two significant digits, where uncertainties typically affect the second digit.

Finally, Table 4 provides selected ancillary data extracted from the published literature. The parameters listed here are described below. Column 2 gives the mass accretion rate onto the star, $\dot{M}_{acc}$. Mass accretion rate determination is based on various methods (e.g., spectrophotometry of veiling of absorption lines due to blue continuum, or also photometry of U band excess in Hartmann et al. 1998, the two methods producing compatible results; similar methods based on UV/optical accretion excess emission also for other references as summarized in Najita et al. 2007; Natta et al. 2006 used Paβ and Brγ lines and compared with other methods). As $\dot{M}_{acc}$ varies among different authors by up to an oder of magnitude or so, we adopted the homogenized accretion rates listed by Najita et al. (2007) or used, as far as possible, values from publications compatible with this compilation (in particular Hartmann et al. 1998). Column 3 gives the equivalent width of the Hα line, $EW(H\alpha)$, and Col. 4 the equivalent width of the [O I] λ6300 line. This line is suspected to originate in jets and outflows, although this interpretation is based on the "high-velocity" component sometimes seen in the line (Hartigan et al. 1995). If such a high-velocity component has been separately measured, we list it in this column, and report the equivalent width of the total flux of the total of the [O I] line in Col. 5 (index t for "total"); we then give, in Col. 6, the logarithm of the [O I] luminosity normalized with the solar luminosity, for the high-velocity component (f). To convert $EW([O I])$ to $L_{[OI]}$, we used the method described by Hartigan et al. (1995) based on the R-band magnitude and the visual extinction; these parameters were taken from the literature or from the SIMBAD database and the 2MASS catalog (Skrutskie et al. 2006). Likewise, in Col. 7 we give the luminosity corresponding to the total flux (t) in the [O I] line, derived from the corresponding EW as above; for some objects, a "wind mass-loss rate" is available in the literature (given in Col. 8), as derived for example from the [O I]$_f$ line flux. We also indicate, in Col. 9, objects for which explicit evidence for jets or outflows has been reported in the literature ("J") and objects classified as having transition disks ("T"). Finally, the

last column (Col. 10) in Table 4 lists references from which these data were obtained (sequentially for the columns in the table), or from which auxiliary parameters such as R-band magnitudes and A_V (for the EW-L conversion) were adopted. Specifically, most values for $\dot{M}_{acc}$ are from Najita et al. (2007) and Hartmann et al. (1998). $EW(H\alpha)$ are mostly taken from Cohen & Kuhi (1979) and Hughes et al. (1994) (the latter for Lupus). For Taurus objects, parameters were extracted from Güdel et al. (2007a) where further references are listed. Information on [O I] equivalent widths and luminosities are mostly from Cohen & Kuhi (1979), Hamann (1994), Hartigan et al. (1995), and Hirth et al. (1997). Most of the mass loss rates, $\dot{M}_{loss}$, are from Hartigan et al. (1995). Although some of the values listed in Table 4 may be given to excessive precision, we prefer leaving the values extracted from the published literature unaltered.

A few notes on individual targets follow: BYB 35 was observed in X-rays but remained undetected. As an approximate extinction is known ($A_J = 5.9$ mag, Gómez & Mardones 2003), we estimated the expected N_H based on the standard interstellar gas-to-dust mass ratio (≈ 100) and dust properties, using $N_H \approx 2 \times 10^{21} A_V$ cm^{-2} and $A_V = 3.6 \times A_J$ (e.g., Vuong et al. 2003). We then adopted a standard X-ray emission model as found for other CTTS in Taurus (see Güdel et al. 2007a for details) to estimate the flux upper limits based on the background count rate in the vicinity of the expected stellar position.

The two targets SSTc2d J182928.2+002257 and SSTc2d J182909.8+003446 were also observed in X-rays but both remained undetected. Given the poorly known properties of these objects and the absence of reliable extinction values to estimate expected N_H values, no reliable upper limits to the X-ray fluxes and luminosities could be calculated.

T Tau S is occasionally defined as a protostar. Although Class I sources are not studied here (see Flaccomio et al. 2009, for such objects), we do include T Tau S, itself a binary, together with T Tau N. The status of T Tau S is not entirely clear – much of the observed extinction/absorption may in fact be due to a thick, near-edge-on disk (Solf & Böhm 1999; Duchêne et al. 2005). Also, T Tau S is the best studied [Ne II] jet source, providing important evidence for the role of outflows in the

Table 5. Sample statistics.

	Number of targets
Sample	92
[Ne II] observations	92
[Ne II] detections	58
[Ne II] non-detections	34
X-ray observations	67
X-ray detections	64[a]
X-ray non-detections	3
[Ne II] & X-ray observations	67
[Ne II] detection & X-ray detection	40[a]
[Ne II] non-detection & X-ray detection	24
[Ne II] detection & X-ray non-detection	1
[Ne II] non-detection & X-ray non-detection	2

Notes. [a] T Tau S included in X-ray detections (for intrinsic L_X)

production of [Ne II] emission. T Tau S has not clearly been detected in X-rays owing to high photoelectric absorption, although marginal excess flux at its position may be present (Güdel et al. 2007c). However, the mass of the more massive component T Tau Sa is very nearly the same as the mass of T Tau N, namely $\approx 2\ M_\odot$ (Köhler et al. 2008). Because X-ray emission of CTTS is correlated with stellar mass (Telleschi et al. 2007b), we assign the same L_X to T Tau Sa as found for T Tau N. This value may be uncertain by a factor of a few but given the outstanding [Ne II] properties of this object, in particular its high [Ne II] luminosity (van Boekel et al. 2009), this uncertainty will not critically influence our results. The X-ray luminosity is in rough agreement with an estimated X-ray luminosity corresponding to the marginal excess flux seen in the *Chandra* HRC image (Güdel et al. 2007c).

DG Tau, DP Tau, and HN Tau show peculiar X-ray spectra with two components subject to different absorbing gas column densities (Güdel et al. 2007b, 2009b). We considered only the hard, coronal component for the X-ray flux, while the soft component is probably associated with the jets. In Sz 102 (= TH 28, or "Krautter's Star"), the entire observed X-ray flux may be related to jets (Güdel et al. 2009b). Its X-ray spectrum is very soft, while the expected near-edge-on geometry should absorb essentially all stellar X-rays or transmit only the hardest portion of the spectrum. We will therefore not consider this star for statistical studies involving L_X.

Table 5 summarizes sample statistics. In total, our sample contains 92 objects, for all of which we derived [Ne II] fluxes or upper limits or found corresponding information in the literature (58 detections and 34 upper limits). X-ray information is available for 67 of these objects, 64 of which were detected. Both [Ne II] and X-ray detections are available for 40 objects. Obviously, ancillary data are far from complete for our sample, and therefore smaller subsets had to be used for specific correlation studies.

4. Data reduction and analysis

For a summary of the analysis strategies for the largest [Ne II] subsample discussed in our paper, see Lahuis et al. (2007). The objects from Spitzer GO program 2030 (AORs 145XXXXX in Table 2) were all reduced according to the procedure described in Carr & Najita (2008).

X-ray data are available from different satellite observatories. We confined our X-ray analysis to data from the CCD detectors on board *XMM-Newton* (Jansen et al. 2001) and the

Chandra X-ray Observatory (*Chandra* henceforth; Weisskopf et al. 1996). Although *ROSAT* observed many of our targets as well, its rather soft bandpass (0.1–2 keV) and its very low spectral resolving power ($E/\Delta E \approx 2$) make a reliable modeling of relatively faint CTTS subject to considerable absorption difficult and uncertain. All *XMM-Newton* and *Chandra* data were consistently reduced and analyzed. The data reduction procedures for *XMM-Newton* data are identical to those described in Güdel et al. (2007a) for objects in Taurus. Whenever possible, we extracted the X-ray spectra from the pn-type *European Photon Imaging Camera* (EPIC-pn; Strüder et al. 2001); if this camera did not provide useful data (e.g., if the target fell into a CCD gap), we used the two spectra extracted from the MOS-type EPIC cameras (Turner et al. 2001). The few *Chandra* spectra were extracted from the *Advanced CCD Imaging Spectrometer* (ACIS), using the so-called events2 files from the archive. Both for *XMM-Newton* and *Chandra*, counts were extracted from circular areas around the source position, and background spectra were defined from nearby, source-free areas on the same CCD chip.

The X-ray spectral interpretation was performed in the XSPEC vers. 11.3.1 software (Arnaud 1996) using simple one- or two-component (in exceptional cases, three-component) optically thin, collisional-equilibrium plasma models, each component being defined by its temperature (T) and emission measure (EM). The element abundances of the plasma were held fixed at values commonly found in pre-main sequence or young active stars (see Güdel et al. 2007a). The spectral model was further subject to photoelectric absorption described by the absorbing gas (equivalent hydrogen) column density, N_H. Fit parameters therefore were T and EM for each component, and N_H in common to all components. We will report only the total X-ray fluxes of our targets and N_H, as these are the most important parameters for theories of [Ne II] emission. Fitted EMs roughly scale with L_X, and temperatures were usually found in the range typical for T Tauri stars (i.e., a few tenths to a few keV, see Güdel et al. 2007a, for the Taurus objects reported here).

5. Results

5.1. Ne II emission from subsamples

We start the presentation of our results by reviewing the range of evolutionary stages and circumstellar environments of our targets. This consideration is motivated by our finding that jets and outflows appear to be important contributors to the [Ne II] emission from young stars.

We have identified 14 objects with some evidence of spatially resolved jets or outflows, defining the subclass of *jet sources*. This classification is purely qualitative (e.g., based on imaging in forbidden lines, or evidence of Herbig-Haro objects) as no effort was made to quantify mass loss rates, shock speeds, or shock excitation in the jets. We do, at this stage, not include objects with indirect evidence for jets, such as strong but spatially unresolved [O I] emission. We will discuss such more quantitative parameters that may be related to outflows in a later step.

Our sample also contains 13 *transition disks* which we study separately. Note that we include different types of transition disks (e.g., Najita et al. 2007). Some of them have low disk masses and are optically thin (at UV and infrared wavelengths) throughout the disk. They are sometimes also called "anemic" disks (Lada et al. 2006). Another class of transition disks are those with a gap or hole in the dust distribution in the inner disk but with a massive optically thick outer disk, sometimes also
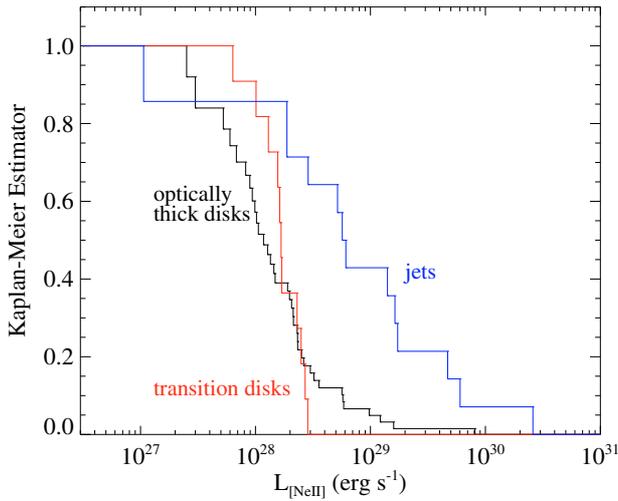
Fig. 1. Kaplan-Meier estimators for $L_{[Ne\,II]}$ for the three subsamples (optically thick disks without jets, transition disks, and jets).

called "cold" disks (Brown et al. 2007). Several cold disks are now known to have residual gas present inside the dust gap (e.g., Pontoppidan et al. 2008; Salyk et al. 2009). Transition disks rarely show jets, making them a relatively homogeneous group without much [Ne II] contamination from jets and outflows, although the level of disk clearance will obviously vary among the objects. CS Cha is exceptional in this group, showing both a transition disk (Espaillat et al. 2007) and signatures of a jet (Takami et al. 2003). We will address this case separately although we will generally include it in the subclass of jets given that jets may largely dominate [Ne II] line emission (see below). We thus define the remainder of our objects as the class of *optically thick disks* without (known) jets (66 objects).

We first study whether the [Ne II] production differs between the above three classes. Figure 1 shows the Kaplan-Meier estimator for the cumulative distribution of $L_{[Ne\,II]}$, including information from upper limits, as calculated in the ASURV statistical software package (Lavalley et al. 1992). For *optically thick disks*, $L_{[Ne\,II]}$ is broadly distributed between 10^{27} erg s^{-1} and 10^{30} erg s^{-1}, with a median at 1.1×10^{28} erg s^{-1}. Interestingly, the distribution seems to be more narrowly confined for the smaller sample of *transition disks* (excluding CS Cha), but it shows nearly the same median, $L_{[Ne\,II]} \approx 1.6 \times 10^{28}$ erg s^{-1}. The distribution is bounded by the maximum luminosity of $\approx 3 \times 10^{28}$ erg s^{-1}. The probability that the two distributions are drawn from the same parent population is 31% (using the Peto-Prentice Generalized Wilcoxon text in ASURV).

In contrast, the *jet sources* show a significantly different distribution shifted to nearly ~tenfold higher luminosities, with a median of 6×10^{28} erg s^{-1}. Here, the probability that this distribution agrees with the distribution of the optically thick disks is 0.01%.

We next seek correlations between $L_{[Ne\,II]}$ and stellar or disk parameters. We will employ linear regression to compute functions of the form $\log L_{[Ne\,II]} = a + b \log x$, but because many objects show upper limits to $L_{[Ne\,II]}$, we will use "survival statistics" that take these values into account. We use the parametric estimation maximization (EM) algorithm in ASURV, which implements methods presented by Isobe et al. (1986). We also use ASURV to compute correlation coefficients for the same samples, specifically using the Cox hazard model, Kendall's tau, and Spearman's rho values (where the latter typically requires

at least 30 entries to be accurate). A summary of our statistical results is given in Table 6.

5.2. [Ne II] emission and X-rays

We first discuss a possible dependence between $L_{[Ne\,II]}$ and the intrinsic, unabsorbed L_X. Figure 2 relates the two quantities for the entire sample, distinguishing between the three object classes (using different symbol shapes and colors), with separate (open) symbols for upper limits (mostly in $L_{[Ne\,II]}$). We provide error bars for $L_{[Ne\,II]}$ as derived from spectral analysis, while for X-rays spectral-fit errors are normally not relevant as the range of uncertainty is dominated by variability on various time scales. Such variability is, apart from singular flares, typically characterized by flux variations within a factor of two from low to high levels. We therefore adopted error bars defining flux deviations of $\sqrt{2}$ to both higher and lower values.

Note the large range now available in both variables, amounting to ≈ 2 dex in L_X and ≈ 3 dex in $L_{[Ne\,II]}$, i.e., much wider ranges than in previous studies (Espaillat et al. 2007; Lahuis et al. 2007; Pascucci et al. 2007). No sharp correlation is found although a statistically significant dependence exists after excluding the four very strong [Ne II] detections (for T Tau S, DG Tau, Sz 102, and EC 82) that define the upper envelope of the distribution (a correlation still exists if they are included). Three of these objects eject prominent jets (T Tau S, DG Tau, and Sz 102) while EC 82 is a little studied object with a relatively strongly absorbed high-inclination/near-edge-on disk (Pontoppidan et al. 2005). The best-fit regression for the remaining sample has a slope of 0.50 ± 0.15, with a low probability, $P \lesssim 6\%$, for this correlation being attained by chance (Table 6).

As indicated above, the transition disks behave like the optically thick disks without jets. The jet sources, in contrast (shown as blue diamonds in Fig. 2 and further figures), are systematically more luminous in [Ne II], revealing only modest overlap with the region occupied by the other objects. A separate regression analysis for the jet sources indicates a significant dependence with a regression slope of 0.77 ± 0.27, i.e., compatible with proportionality. The dependence is less tight for the non-jet objects although still significant, with a shallower slope of 0.51 ± 0.14. This trend is shallower than what simple theories would predict, i.e. trends close to proportionality (Meijerink et al. 2008; Hollenbach & Gorti 2009, see Sect. 6.1).

5.3. [Ne II] emission and accretion

Figure 3 relates $L_{[Ne\,II]}$ to the mass accretion rate, as suggested by Espaillat et al. (2007). Again, a large range of $\dot{M}_{acc}$ values is covered, spanning the interval of $\approx 10^{-10} - 10^{-6}$ $M_\odot$ yr^{-1}. No correlation is evident among the jet sources or the disks without jets separately, with $P \approx 18-79\%$. However, stronger accretors are predominantly jet sources, and they reveal higher $L_{[Ne\,II]}$.

A dependence between the two variables is therefore ambiguous. Although a physical dependence may be absent, the segregation into objects with and without jets may produce an apparent correlation. Jet engines are typically younger and more active objects, and given a rough correlation between accretion rate and outflow rate (e.g., Hartigan et al. 1995), jet sources typically also show high accretion rates. Our separate finding that jet sources are generally more luminous [Ne II] sources thus may in fact produce a *bi-modal distribution* rather than a correlation based on any physical dependence.

Table 6. Correlation summary.

Parameter	# points	# upper limits	P(Cox Hazard)	P(Kendall tau)	P(Spearman rho)	Slope	Intercept
$\log L_{X,0.3-10,\text{unabs}}{}^a$	60	24	**0.016**	*0.055*	*0.059*	0.50 ± 0.15	12.99
only jets[a]	12	2	**0.015**	**0.027**	**0.037**	0.77 ± 0.27	5.75
without jets[a]	50	22	**0.011**	**0.043**	*0.056*	0.51 ± 0.14	12.77
$\log L_{X,0.3-10,\text{abs}}{}^a$	60	24	**0.020**	**0.029**	**0.050**	0.51 ± 0.17	13.02
only jets[a]	12	2	**0.031**	**0.041**	*0.076*	0.78 ± 0.26	5.84
without jets[a]	50	22	**0.022**	*0.072*	*0.091*	0.44 ± 0.18	15.06
$\log \dot{M}_{\text{acc}}$	36	9	0.273	**0.037**	**0.046**	0.35 ± 0.11	31.14
only jets	12	2	0.789	0.782	0.637	0.28 ± 0.27	30.90
without jets	24	7	0.181	0.639	0.717	-0.05 ± 0.07	27.70
$\log(\dot{M}_{\text{acc}} L_X)$	33	9	*0.053*	**0.012**	**0.021**	0.44 ± 0.10	18.59
only jets	11	2	*0.080*	*0.059*	**0.048**	0.45 ± 0.16	18.51
without jets	22	7	0.431	0.942	0.934	-0.02 ± 0.09	28.66
$EW(\text{H}\alpha)$	55	18	0.470	0.223	0.293	0.26 ± 0.18	27.82
only jets	12	2	0.605	0.836	0.789	0.11 ± 0.55	28.63
without jets	43	16	0.596	0.889	0.804	-0.04 ± 0.14	28.15
$EW(\text{O\,I}_l)$	31	9	**0.004**	**0.008**	**0.007**	0.66 ± 0.17	28.37
$EW(\text{O\,I}_l) L_X$	25	8	**0.002**	**0.003**	**0.009**	0.78 ± 0.15	5.01
$EW(\text{O\,I}_f)$	17	4	*0.091*	0.139	0.137	0.35 ± 0.13	28.49
$EW(\text{O\,I}_f) L_X$	16	4	0.121	0.118	0.140	0.45 ± 0.16	15.15
$\log L_{\text{OI}_l}$	28	8	**0.015**	**0.025**	**0.034**	0.42 ± 0.10	29.72
$\log(L_{\text{OI}_l} L_X)$	24	7	**0.007**	**0.015**	**0.027**	0.46 ± 0.10	16.47
$\log L_{\text{OI}_f}$	17	4	0.208	0.139	0.176	0.23 ± 0.09	29.41
$\log(L_{\text{OI}_f} L_X)$	16	4	0.179	0.118	0.137	0.33 ± 0.12	20.03
$\log \dot{M}_{\text{loss}}$	13	3	0.110	*0.067*	*0.100*	0.44 ± 0.14	32.06
$\log(\dot{M}_{\text{loss}} L_X)$	12	3	*0.088*	0.215	0.263	0.46 ± 0.13	18.48
$\log N_{\text{H}}$	64	24	0.206	0.157	0.192	0.28 ± 0.18	28.35
$\log(N_{\text{H}} L_X)^a$	60	24	*0.051*	0.104	0.126	0.27 ± 0.10	20.18

Notes. [a] Four high-$L_{[\text{Ne\,II}]}$ objects have not been considered for these correlations, namely T Tau S, DG Tau, EC 82, and Sz 102 (see text and figures for details). Sz 102 has not been considered in any of the correlations that involve L_X.
The number of points ("# points") includes upper limits, detailed in the column "# upper limits".
L_X refers to $L_{X,0.3-10,\text{unabs}}$. P is the probability that the correlation is obtained by chance. P values up to 5% and between 5% and 10% are printed in boldface and italics, respectively.

We have also correlated $L_{[\text{Ne\,II}]}$ with the equivalent width of the Hα line (an accretion indicator, Table 4), but found no significant trend (Table 6).

5.4. [Ne II] emission and [O I] emission

Motivated by the systematic difference between $L_{[\text{Ne\,II}]}$ for jet sources and objects without jets, we now introduce parameters that diagnose – possibly among other things – mass loss, namely the equivalent width and the luminosity of the [O I] $\lambda6300$ line. We first study whether [O I] and [Ne II] emission correlate in a general way, regardless of their origin, perhaps suggesting that they are diagnostic lines of *the same* emission regions. We indeed find a significant correlation ($P \lesssim 3\%$) between the respective luminosities (Fig. 4, Table 6).

Although the subsamples in consideration are naturally dominated by stars with strong mass loss, i.e., objects with jets, many further CTTS show spectroscopic evidence for [O I] emission, perhaps resulting from small, spatially unresolved jets (Hartigan et al. 1995; Hirth et al. 1997) but also from disk surface layers (Hartigan et al. 1995; Acke et al. 2005; Meijerink et al. 2008).

5.5. [Ne II] emission and mass loss indicators

The origin of [O I] $\lambda6300$ line emission is ambiguous; the low-velocity component has been interpreted as being formed at the disk surface, in analogy to [Ne II] emission (Hartigan et al. 1995; Acke et al. 2005; Meijerink et al. 2008). For this low-velocity component, thus, a correlation between [Ne II] and [O I] luminosities would directly support the disk emission model for [Ne II]. The high-velocity component is – less ambiguously – ascribed to a jet (Hartigan et al. 1995; Hirth et al. 1997). Again, a correlation would support a model in which shocks or X-ray irradiation from the star excite the [Ne II] line in the jet gas. The statistics at hand is, unfortunately, insufficient to draw convincing conclusions with respect to correlations with the [Ne II] luminosity.

We plot in Fig. 5 $L_{[\text{Ne\,II}]}$ against the mass loss rate, $\dot{M}_{\text{loss}}$, as determined from [O I] luminosities (Hartigan et al. 1995). There is a clear trend (at the 10% probability level, see Table 6), further supporting our view that jets define a separate class of [Ne II] emitters. The trend suggests that the [Ne II] luminosity increases with increasing mass loss although the relation is non-linear (exponent of $\approx 0.4-0.5$, see Table 6).

### 5.6. [Ne II] emission and the gaseous environment of CTTS

Although we exclude Class I sources from consideration in this work, many CTTS/Class II sources show signs of excessive absorption (in X-rays) and extinction (in the optical) compared to weak-lined T Tauri stars (WTTS)/Class III objects. For the XEST survey of the Taurus Molecular Cloud the visual extinction, A_V, is larger by ≈ 1 mag for CTTS compared to WTTS (median; ≈ 2 mag for the mean), where the median A_V for WTTS is ≈ 0.9 mag. There are several possible explanations for this result: i) CTTS are predominantly located in denser regions of
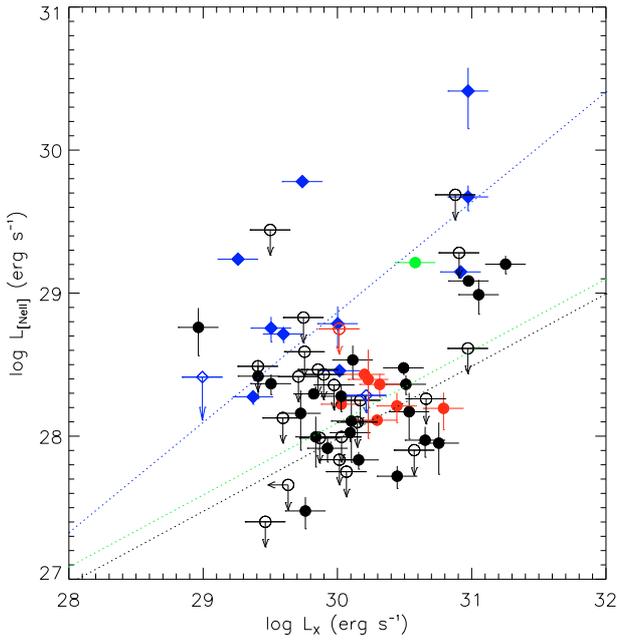
Fig. 2. log $L_{[\text{Ne II}]}$ vs. log L_X. Black circles refer to optically thick disks without jets, red circles to transition disks, and blue diamonds to jet sources. The green circle marks the position of CS Cha, a transition disk with a jet. Filled and open symbols refer to detections and non-detections, respectively. Error bars comprise a factor of 2 for X-rays (typical for the range of variability), but represent the actual measurement and fit uncertainties for $L_{[\text{Ne II}]}$. Regression lines are given for the entire sample (green) and also separately for the non-jet objects (black, including transition disks) and the jets (blue). Four objects defining the upper envelope of the distribution have been excluded from the regression analysis of the *combined sample*, namely T Tau S, DG Tau, EC 82, and Sz 102.
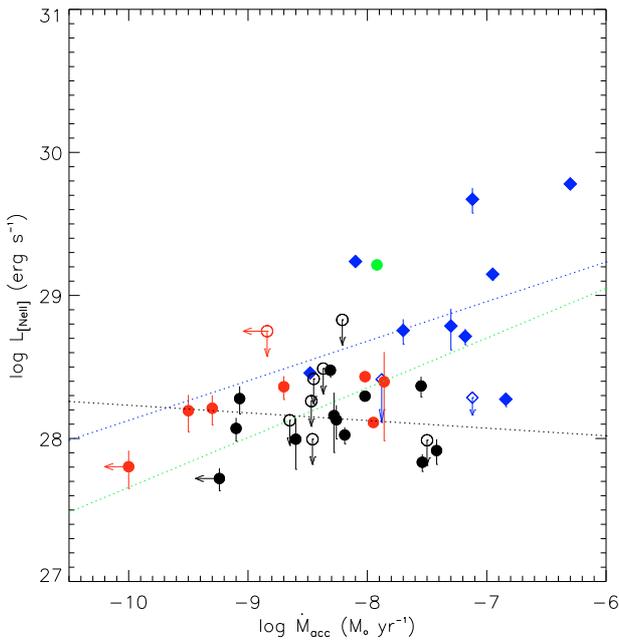
Fig. 3. log $L_{[\text{Ne II}]}$ vs. log $\dot{M}_{\text{acc}}$. Symbols, lines and colors are as in Fig. 2. Regression analysis excludes the upper limits to $\dot{M}_{\text{acc}}$ for CoKu Tau 4, DoAr 25, and SR 21.
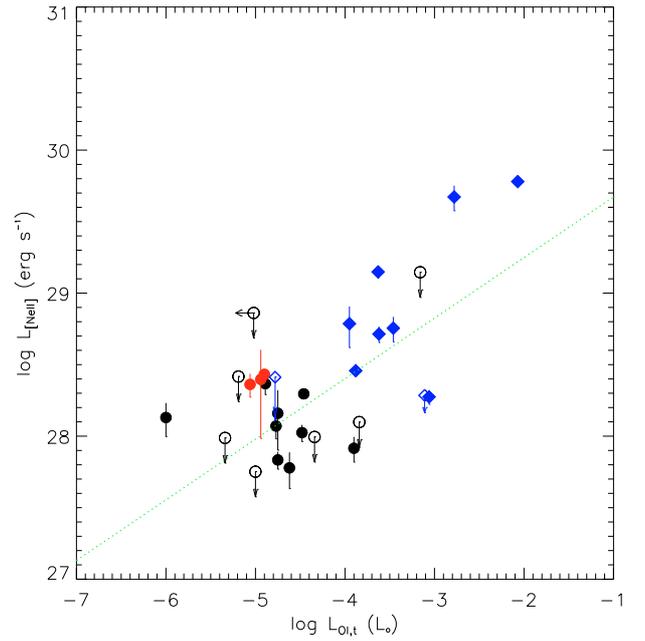

Fig. 4. log $L_{[\text{Ne II}]}$ vs. log $L_{[\text{O I}],t}$ for the entire [O I] line flux. The upper limits to log $L_{[\text{O I}],t}$ for HT Lup has been excluded from the regression fit. Symbols, lines and colors are as in Fig. 2.
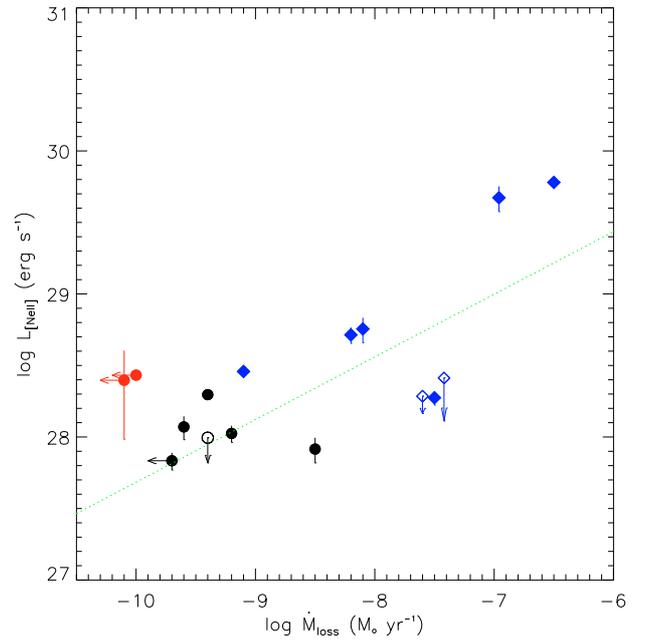
Fig. 5. log $L_{[\text{Ne II}]}$ vs. $\dot{M}_{\text{loss}}$. For the regression analysis, objects with upper limits in $\dot{M}_{\text{loss}}$, namely BP Tau, FM Tau, V836 Tau, GM Aur, were not considered. Symbols, lines and colors are as in Fig. 2.

the surrounding molecular cloud; ii) there is more residual gas in the immediate vicinity of the star. Additional extinction may arise from iii) stronger dusty stellar winds and disk winds; iv) from the disk itself; or from v) dusty accretion flows. Point iv) is clearly important for near-edge-on disks, with lines-of-sight traversing the upper disk layers (e.g., Kastner et al. 2005); such orientation is, however, rare. Point (v) is probably less relevant given high temperatures in the the disk-star accretion flows,
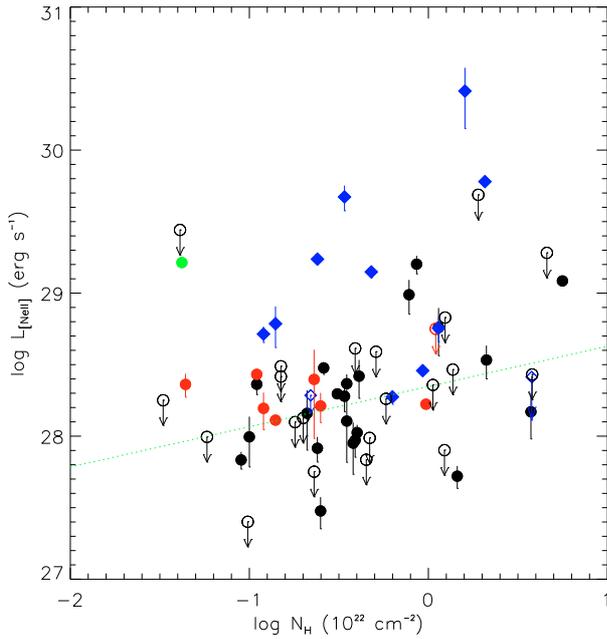
Fig. 6. log $L_{[\text{Ne II}]}$ vs. log N_H as determined from X-ray spectral observations along the line of sight to the star. Symbols, lines and colors are as in Fig. 2.

resulting in largely dust-depleted gas which is still capable of absorbing X-rays (see Sect. 6 below).

Studying [Ne II] emission in the context of extinction or X-ray photoelectric absorption may provide important hints on its origin. On the one hand, higher levels of gas in the immediate stellar environment absorb more EUV and X-ray flux, thus suppressing formation of Ne^+ in the surface layers of the circumstellar disks. In extreme cases, no EUV or X-ray radiation may reach the disk surface – see Sect. 6. On the other hand, [Ne II] may be formed in the absorbing layer itself, which would be suggested if $L_{[\text{Ne II}]}$ increases with increasing gas columns.

In Fig. 6, we plot $L_{[\text{Ne II}]}$ vs. the X-ray derived N_H along the line-of-sight to the stellar X-ray source. We find a weak but hardly significant trend toward higher $L_{[\text{Ne II}]}$ with increasing N_H.

Because the effect of N_H is to lower the X-ray flux that reaches a circumstellar disk, we can also ask whether $L_{[\text{Ne II}]}$ correlates with the X-ray flux *behind the absorbing medium*, i.e., the "attenuated flux". This flux is difficult to determine as the absorbing gas column that X-rays or EUV photons encounter *toward the disk surface* is unknown. However, we do know the attenuated flux reaching the observer. Using the observed, attenuated L_X and assuming that the latter is, on average, in some ways related with the attenuation between the star and the [Ne II] emitting source, the result is very similar to what we derived for the intrinsic luminosities in Fig. 2, not permitting further conclusions.

5.7. [Ne II] emission and the role of L_X

The leading models for [Ne II] production posit that the X-ray or EUV flux ionizes and excites Ne. We therefore also test whether $L_{[\text{Ne II}]}$ may depend on some ad hoc products between L_X and the parameters related to the [Ne II] emission source. Figure 7 shows two examples for the products of L_X with $L_{[\text{O I}],t}$, and $\dot{M}_{\text{loss}}$. The quality of the correlations remains similar (Table 6).
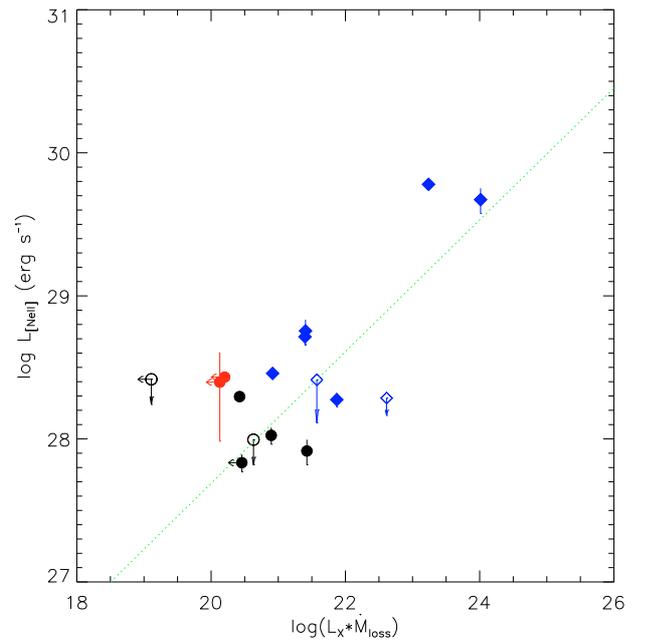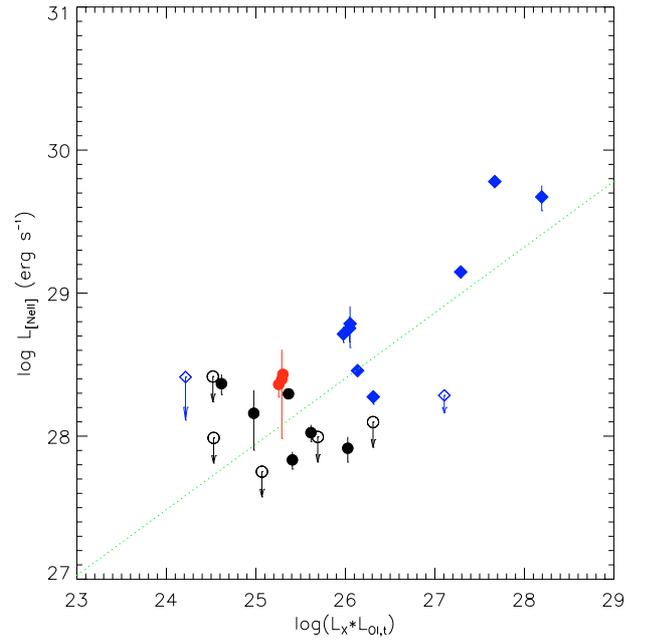
Fig. 7. log $L_{[\text{Ne II}]}$ vs. the logarithm of the product of L_X times $L_{[\text{O I}],t}$ (*upper*) and $\dot{M}_{\text{loss}}$ (*lower*). For the regression analysis, objects with upper limits in $\dot{M}_{\text{loss}}$, namely BP Tau, FM Tau, V836 Tau, GM Aur, were not considered. Similarly, the upper limit to log $L_{[\text{O I}],t}$ for HT Lup have been excluded from the regression fit analysis. Symbols, lines and colors are as in Fig. 2.

6. Discussion

We suggest (as in Güdel et al. 2009a) four potential [Ne II] emission regions in stellar environments, partly supported by previous work:

– disk surface layers irradiated by EUV or X-rays, or heated by accretion shocks; this model has been favored by initial theoretical work (Glassgold et al. 2007);

- photoevaporative flows above the disk surface, as suggested by Herczeg et al. (2007) and modeled by Alexander (2008);
- jets, as suggested from a statistical sample more thoroughly discussed in the present paper, and from explicit observations of the T Tauri triple (van Boekel et al. 2009); both X-ray induced and shock-induced [Ne II] flux production is possible;
- absorbing accretion columns close to the star.

We now discuss our results in the context of these emission models.

6.1. [Ne II] emission from disk surface layers

Heating and ionization of gaseous disk surface layers by stellar X-rays or EUV photons has defined a leading theory of [Ne II] production, as initially suggested by Glassgold et al. (2007) and followed up by Ercolano et al. (2008), Meijerink et al. (2008), and Hollenbach & Gorti (2009). Ne^+ (and Ne^{++}) are either produced by ejection of a K-shell or an L-shell electron after absorption of an X-ray photon in weakly ionized, X-ray heated gas with temperatures of a few 1000 K (Glassgold et al. 2007) or are collisionally ionized in a hot, strongly ionized ($\approx 10^4$ K) "H II" region formed at the disk surface after irradiation by EUV photons (Gorti & Hollenbach 2008; Hollenbach & Gorti 2009).

Glassgold et al. (2007) estimated [Ne II] fluxes for two disk models in which either mechanical heating or X-ray heating is dominant, with a stellar $L_X = 2 \times 10^{30}$ erg s^{-1}, predicting typical fluxes of 10^{-14} erg cm^{-2} s^{-1} at a distance of 140 pc, or $\log L_{[Ne II]} \approx 28.4$. Such luminosities compare very favorably with the bulk of our distribution, although the most extreme [Ne II] luminosities exceed this level by up to two orders of magnitude.

These calculations were extended by Meijerink et al. (2008) to include various stellar L_X values, $L_{[Ne II]}$ being derived from the integrated emissivities across the entire disk for the case of dominant X-ray heating. Although the authors mention that their models should not be used to suggest a general correlation between the two parameters as the disk properties have been held fixed, these models provide a guide to what can be expected for similar disks. Their model trend is overplotted in Fig. 8 (dashed green line). It indeed does provide a good description of the [Ne II] luminosity level for the optically thick disks, although the slope of the observed trend is not reproduced, and the jet-driving stars show a much higher $L_{[Ne II]}$ than the models.

Ercolano et al. (2008) estimated $L_{[Ne II]} \approx 8.7 \times 10^{-7} L_\odot$ or $\log L_{[Ne II]} \approx 27.5$ based on radiative transfer calculations assuming $L_X = 2 \times 10^{30}$ erg s^{-1}. Although this value is lower than observed at this L_X (see Fig. 8), it matches $\log L_{[Ne II]}$ of some of the fainter objects in our sample. These models were extended to include variations in X-ray spectral hardness and also disk flaring (Schisano et al. 2010). Disk flaring was modeled by adapting values typically observed in dust disks, but also by calculating the hydrostatic, flaring disk structure self-consistently for the gas component. These calculations demonstrate that disk flaring is of utmost importance (given the largely increasing cross section of a strongly flared disk). Also depending on the spectral hardness (based on an *absorbed* X-ray spectrum), characteristic values for $\log L_{[Ne II]}$ are 2×10^{26}–3×10^{27} erg s^{-1} for $L_X = 2 \times 10^{29}$ erg s^{-1}, 1×10^{27}–3×10^{28} erg s^{-1} for $L_X = 2 \times 10^{30}$ erg s^{-1}, 2×10^{28}–3×10^{30} erg s^{-1} for $L_X = 2 \times 10^{31}$ erg s^{-1} (see Fig. 8). Such values again compare favorably with the *optically thick* disk sample except for the most [Ne II] luminous objects among them, as already pointed out by Schisano (2010).
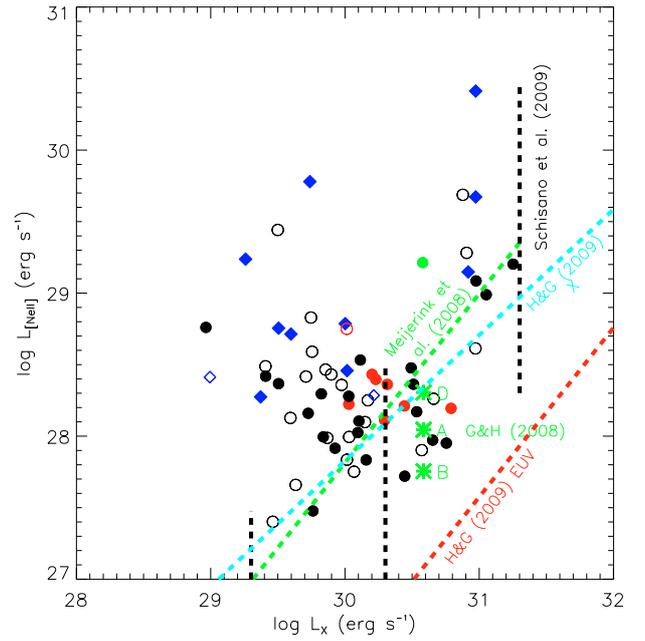
Fig. 8. Same as Fig. 2, but model predictions for [Ne II] disk emission are overplotted, based on Meijerink et al. (2008) for a fixed disk (green dashed line), Gorti & Hollenbach (2008) (three green stars), Schisano et al. (2010) (vertical dashed black lines), and Hollenbach & Gorti (2009) (dashed cyan line for X-ray layer, dashed red line for EUV layer).

Gorti & Hollenbach (2008) presented calculations of [Ne II] emission from optically thick disks irradiated by UV, EUV, and X-rays (with similar luminosities in each band, $\approx 10^{-3} L_\odot$; model "A"). Variants involved a 100 times lower dust opacity (representing an evolved disk, model "B"), absence of X-rays (model "C"), and a tenfold higher FUV luminosity (model "D"). The resulting total $L_{[Ne II]}$ are plotted for models A, B, and D in Fig. 8, and once again they match the fainter [Ne II] fluxes from optically thick disks quite well.

Hollenbach & Gorti (2009) estimate the total [Ne II] flux both from the EUV-heated H II disk surface layer and the X-ray heated subsurface layer to find that for plausible stellar EUV and X-ray spectra, the X-ray layer produces $\approx$ twice as much $L_{[Ne II]}$ for equal total luminosities in both bands, simply because of the much smaller column available to EUV, given the strong absorption by H and He. The numerically calculated $L_{[Ne II]}$ values compare well with values from other authors discussed above, showing a near-linear increase with L_X or L_{EUV}, see Fig. 8, the emission mostly originating from within 10 AU of the star. The authors also compute [O I] $\lambda 6300$ luminosities from the EUV and X-ray heated disk layers, concluding, however, that typical luminosities remain orders of magnitude lower ($\lesssim 10^{-6} L_\odot$ to a maximum of $10^{-4} L_\odot$) than strong [O I] luminosities observed in many CTTS ($10^{-6} L_\odot$–$10^{-3} L_\odot$, referring to the so-called low-velocity component that has been attributed to disk emission; Hartigan et al. 1995).

In summary, most of the model calculations described above yield $L_{[Ne II]}$ of the same order as observed for the *optically thick* disk sample, with a tendency for somewhat higher *observed* luminosities especially for $L_X \lesssim 10^{30}$ erg s^{-1}. We suggest that further features that might enhance [Ne II] emission are puffed-up disks as well as actively photoevaporating disks, because a larger fraction of the X-rays (or EUV radiation) would be absorbed to

subsequently produce [Ne II] emission. There is indeed evidence that [Ne II] emission may come from a disk-related photoevaporative flow, suggested by small but non-zero radial velocities measured as a slight blue-shift of the [Ne II] line (Pascucci & Sterzik 2009).

6.2. Circumstellar absorption: Do X-rays/EUV reach the disk?

In the light of the presence of various gaseous components in the immediate stellar vicinity such as accretion columns, disk atmospheres, X-winds, or photoevaporative flows, a critical question emerges on whether high-energy photons from the star in fact reach the disk surface. This problem has been addressed by Hollenbach & Gorti (2009) who present both analytic estimates and numerical results from a geometrically self-consistent disk model shielded by an outflowing wind. Observationally, the mass loss rates of such winds scale as $\approx \dot{M}_{acc}$ (e.g., Hartigan et al. 1995; White & Hillenbrand 2004) and therefore set limits to the penetration of stellar FUV, EUV, and X-ray photons to the disk surface. Specifically, the authors estimate that FUV and 1 keV X-ray photons penetrate the wind for $\dot{M}_{acc} \lesssim 4 \times 10^{-7}\ M_\odot\ yr^{-1}$, while softer X-rays and EUV photons require $\dot{M}_{acc} \lesssim 8 \times 10^{-9}\ M_\odot\ yr^{-1}$. If [Ne II] emission is induced by soft X-ray or EUV irradiation of the disk, then obviously winds, and by implication accretion rates, must be sufficiently modest. Many of our sources, in particular those ejecting jets, violate these conditions, i.e., disk [Ne II] emission is unlikely in these cases, at least if soft X-rays or EUV radiation are responsible for the excitation.

What is the observational evidence? As mentioned earlier, the absorbing gas column between the X-ray/EUV emitting corona (or accretion spots) and the disk surface is generally unknown but columns are well measured along the line of sight to the observer. Again assuming that the latter columns on average reflect approximately the values toward the disk, we plot in Fig. 9 the X-ray determined N_H against the stellar mass accretion rate $\dot{M}_{acc}$. Two samples have been used, namely stars from the present work (in blue) and CTTS from the XEST Taurus X-ray survey (Güdel et al. 2007a) (in black). Upper limits to N_H are given by arrows; data for a few objects for which the spectral fit converged to $N_H = 0$ were dropped from consideration. The two samples show a similar distribution; more importantly, both suggest an increasing trend for N_H with increasing $\dot{M}_{acc}$ although – expectedly – with considerable scatter. The trend adopted by Hollenbach & Gorti (2009) is shown by a thin line; it is obviously too low for N_H by about an order of magnitude but otherwise reflects the observed trend well.

Part of the absorption is due to the large-scale gas distribution in the star-forming regions and also interstellar gas along the line of sight. Because CTTS are systematically more absorbed (or visually extincted) than WTTS (Güdel et al. 2007a), we propose that the excess absorption is due to gas in the immediate stellar environment of CTTS, such as accretion flows or disk winds. The average of $\log N_H$ for WTTS in Taurus is shown by the horizontal line in Fig. 9, corresponding to $N_H = 1.7 \times 10^{21}\ cm^{-2}$ (with a standard deviation of the N_H distribution of 0.44 dex). Clearly, apart from some scatter, almost all CTTS show N_H around that value or higher. For N_H close to the WTTS level, we cannot determine its origin but for higher N_H, we suggest that circumstellar material adds to the absorption.

Figure 9 also shows the critical values of N_H for which X-rays are attenuated by a factor of e, i.e., the optical depth unity, for the three photon energies of 0.1 keV, 0.3 keV, and
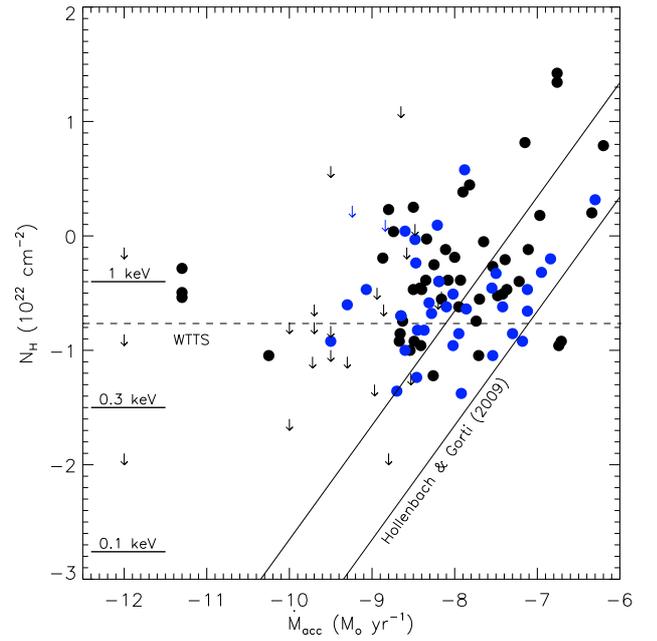
Fig. 9. N_H vs. $\dot{M}_{acc}$ for CTTS in the present sample (blue symbols) and from the XEST survey (black symbols; Güdel et al. 2007a). Measurements are shown by bullets, while upper limits to N_H are given by arrows. The thin diagonal line shows a relation adopted by Hollenbach & Gorti (2009) for an accretion-driven wind, while the thicker, parallel line shows the same relation shifted upward by a factor of ten. The dotted horizontal line shows the (logarithmically) averaged N_H for WTTS in Taurus, and the three short bars on the left indicate optical depth unity for photons with energies of 0.1 keV, 0.3 keV, and 1 keV.

1 keV (shown by horizontal bars). For CTTS with excess N_H, it is clear that EUV radiation is very strongly attenuated, and even soft X-rays of a few times 0.1 keV cannot reach the disk. For most of these stars, even 1 keV photons are severely attenuated.

We thus conclude that the most likely high-energy photons reaching the disk and potentially exciting the [Ne II] line are X-ray photons around 1 keV or higher, and that EUV photons are unlikely to reach any part of the disk, at least for the sample of CTTS that show excess N_H compared to WTTS. This conclusion would be invalid if a photoevaporative flow outside the [Ne II] producing region is responsible for the absorption; however, calculations by Ercolano et al. (2009) show that X-ray driven photoevaporative winds are concentrated in the inner disk, with surface mass-loss rates peaking within 10 AU where [Ne II] emission should be most efficient (Hollenbach & Gorti 2009). Similarly, X-winds and accretion flows would absorb photons at radii within the [Ne II] emitting disk region.

Of course, excess absorption in CTTS may turn the absorbing gas itself into an efficient source of [Ne II] emission as long as the density remains sufficiently low. Testing this hypothesis is, in principle, simple. If the absorbing gas itself were a major source of [Ne II] emission, then $L_{[Ne II]}$ should increase with N_H or also with $L_X N_H$ (with the caveat that excessive N_H may in some cases be due to the disk itself). Although such a trend is present, it is not significant (Table 6).

If X-ray and EUV absorption is important but [Ne II] is still predominantly produced by disk irradiation, then we would expect that $L_{[Ne II]}$ correlates more closely with the attenuated L_X than with the intrinsic L_X, although we recall the caveat that the

observed absorption along our line of sight may differ from the absorption between the star and the disk. Furthermore, [Ne II] production should *decrease* with increasing N_H. These two effects have not been significantly measured (Table 6).

In the most extreme cases, accretion flows shield the circumstellar environment from X-ray or EUV irradiation. This is particularly evident in strongly accreting sources with X-ray jets as discussed above. In these cases, it is unlikely that X-ray/EUV photons reach the disk in significant numbers. The origin of the very strong [Ne II] emission in these sources remains ambiguous because they all eject jets that can be very strong [Ne II] emitters (van Boekel et al. 2009), but massive, low-density accretion flows attenuating the X-ray emission may contribute to [Ne II] emission as well.

6.3. [Ne II] emission from jets

One of the principal results of the present study is the evident [Ne II] excess in stars with jets, as previously suggested by Güdel et al. (2009a) and exemplified by the study of the T Tau triplet by van Boekel et al. (2009). We have been careful not to confuse our sample with strong jets from Class I sources in which other mechanisms (excitation of [Ne II] in the envelope, stronger accretion shocks from material falling onto the disk, etc) may dominate. On the other hand, jets may also contribute to the generally high level of [Ne II] emission seen in Class I sources reported by Flaccomio et al. (2009). Most of our objects are ordinary CTTS although some extreme cases, such as the flat-spectrum source DG Tau or the strongly absorbed (by a near-edge-on thick disk) T Tau S have been included. Figure 6 shows that the distribution of N_H is very similar for the jet sources and the optically thick disks without jets (the same is also true for the transition disks).

What [Ne II] emission can be expected from jets? We briefly discuss three principal [Ne II] formation mechanisms, namely from jet shocks, from irradiation of jets by stellar X-rays or EUV flux, and from X-ray emission produced by the jets themselves.

Jet gas is typically heated to 10^4 K by shocks, shock velocities being a few tens of km s^{-1} (Lavalley-Fouquet et al. 2000). Hollenbach & Gorti (2009) estimate $L_{[Ne II]}$ from fast ($\gtrsim 100$ km s^{-1}) shocks based on results from Hollenbach & McKee (1989), to find a linear relation between $L_{[Ne II]}$ and $\dot{M}_{acc}$ (the latter assumed to scale linearly with $\dot{M}_{loss}$; see Fig. 10). For typical wind/jet velocities, densities, and mass loss rates, they find much higher $L_{[Ne II]}$ than expected from irradiated disks, fully compatible with our findings of very high $L_{[Ne II]}$ in almost all jet sources.

Jets may also be irradiated by stellar X-rays similar to disk surfaces, and may thus be ionized and heated to produce [Ne II] emission. Jet irradiation by stellar X-rays is relatively straightforward because jets move through wide polar cavities evacuated of much of the circumstellar gas (Momose et al. 1996). Evidence for very low gas column densities around CTTS jets has been found from jets that are themselves X-ray sources (see below) and show very low X-ray attenuation despite the presence of appreciable amounts of circumstellar material in other directions (Güdel et al. 2007b). For the T Tauri system, a simple estimate of X-ray induced [Ne II] line excitation across a lightly absorbing gas column showed that the observed stellar L_X may indeed yield the observed [Ne II] fluxes out to a few arcsec from the star (Güdel et al. 2009a).

A rather unexpected finding are CTTS jets that produce X-rays themselves (Güdel et al. 2007b, 2008). Apart from direct X-ray imaging of jets (in particular the case of DG Tau), such jets have also been identified spectroscopically in X-rays.
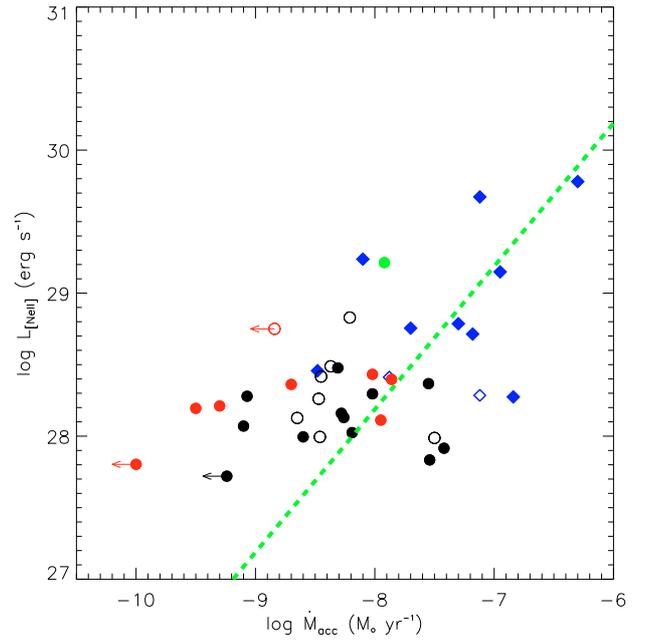
Fig. 10. Same as Fig. 3, but model prediction for [Ne II] jet shock emission is overplotted (dashed green line), referring to calculations by Hollenbach & Gorti (2009) for $\dot{M}_{loss} = 0.1 \, \dot{M}_{acc}$ and all jet gas passing through a shock with a shock velocity >100 km s^{-1} and pre-shock density <10^4 cm^{-3}.

Their anomalous spectra show a highly absorbed, hard and variable coronal component together with a soft, very weakly absorbed and non-variable component apparently produced by the jets close to the star. The excessive absorption of the coronal component is an order of magnitude larger than expected from the visual extinction of the stellar light if standard gas-to-dust mass ratios are assumed. This has been interpreted as being due to dust-depleted accretion streams falling from the disk to the star, thus absorbing X-rays from the underlying corona (Güdel et al. 2007b). It is possible that in these cases the soft jet component is discernible simply because the stellar component is absorbed at low X-ray energies, while in less strongly accreting (and therefore less absorbed) objects the jet component is outshone by the coronal spectrum. Four objects in our sample have been interpreted as showing soft X-ray jets: DG Tau, DP Tau, HN Tau, and also Sz 102, the latter revealing only a soft component, the hard component possibly being completely absorbed by a near-edge-on disk (Güdel et al. 2009b).

Three of these objects show very high $L_{[Ne II]}$, while for DP Tau an upper limit is available. We find no specific trend for the four objects tighter than what is shown in Figs. 2–4. However, except for Sz 102 where only a soft component is present, we have adopted the hard component as representing the stellar radiation. The luminosities in the *soft* components are, 9.6×10^{28} erg s^{-1}, 1.5×10^{29} erg s^{-1}, 4.0×10^{27} erg s^{-1}, and 8.9×10^{28} erg s^{-1} for DG Tau, HN Tau, DP Tau, and Sz 102, respectively (see Güdel et al. 2009b, and this paper for Sz 102). The corresponding $L_{[Ne II]}$ values are, respectively, 6.1×10^{29} erg s^{-1}, 5.6×10^{28} erg s^{-1}, <2.6×10^{28} erg s^{-1}, and 1.7×10^{29} erg s^{-1}, not suggesting any correlation. However, it may be interesting to note that $\dot{M}_{loss} L_{X,soft} = (30, 1.2, < 0.15) \times 10^{21}$ $M_\odot$ yr^{-1} erg s^{-1} for DG Tau, HN Tau, and DP Tau, respectively, which roughly correlates with $L_{[O I],f} = (24, 0.6, 0.06) \times 10^{30}$ erg s^{-1} and with

$L_{\text{[Ne\,II]}} = (61, 5.6, < 2.6) \times 10^{28}$ erg s^{-1} although the statistics are too small for significant conclusions. Although jets may produce both [Ne II] emission and very soft X-rays independently by shock heating, the latter may also contribute to ionization and heating of the predominantly cool jet gas locally, thus adding to [Ne II] emission.

Our finding that [Ne II] emission is enhanced in CTTS with jets, supported by spatially resolved [Ne II] emission from the T Tau jet system (van Boekel et al. 2009), finds a parallel in observations of infrared rovibrational H$_2$ emission from similar targets. The H$_2$ $v = 1 - 0\ S(1)$ line at 2.12 μm shares excitation conditions with [Ne II], i.e., excitation in warm gas heated by UV, X-rays, or shocks, where emission from the disk gas is expected to be confined within 30–50 AU (Beck et al. 2008, and references therein). H$_2$ rovibrational emission has been detected from many CTTS, but again, the emission source is often resolved. In the Beck et al. (2008) high-resolution study of six CTTS (including DG Tau, T Tau, and RW Aur from our sample), the H$_2$ emission morphologies, its detection beyond 50 AU from the star, excitation temperatures exceeding 1800 K, kinematics measureed in the features, and the consistency with calculated shock models suggest that the bulk of the H$_2$ emission is shock-excited emission from jets and outflows rather than emission from disk gas excited by short-wavelength flux from the central star. A comparison of their H$_2$ map of the T Tau system with the spatial distribution of [Ne II] emission reported by van Boekel et al. (2009) indeed suggests some common emission sources.

On the other hand, our finding of a correlation between [Ne II] luminosity and stellar X-ray luminosity specifically for objects with jets suggests an important role of the stellar short-wavelength radiation in exciting [Ne II] in the jet gas, at least relatively close to the star (see also estimates in van Boekel et al. 2009 for the jet system in T Tau detected in [Ne II] out to about 2 arcsec). Explicit theoretical calculations by Shang et al. (2010) for the X-wind model of a YSO jet irradiated by X-rays supports this conclusion further.

6.4. Caveats

Our correlations show systematic scatter of typically an order of magnitude in $L_{\text{[Ne\,II]}}$, regardless of the parameter against which the latter is plotted. Although some stellar or disk parameters, such as L_X or $\dot{M}_{\text{acc}}$ are themselves subject to considerable measurement error, the scatter in $L_{\text{[Ne\,II]}}$ clearly requires further systematic effects. One possibility is that several parameters considered here matter in concert. We have specifically investigated the correlations with the product of some parameters with L_X in an attempt to show that X-ray irradiation is one important factor to produce [Ne II] emission. No decisive improvement of the correlations was found, however.

On the other hand, we have ignored a number of parameters that may influence [Ne II] emission. In particular, we have not considered disk flaring which can increase the cross section area for stellar X-rays considerably. Numerical simulations indeed show order-of-magnitude variations as a result of varying disk flaring for otherwise constant stellar and disk parameters (Schisano et al. 2010). Another factor is the spectral energy distribution of the ionizing and heating X-ray source. Again, accurate measurement of the irradiating spectrum is not possible although the intrinsic stellar X-ray spectrum can be reconstructed from observations. X-ray spectral hardness indeed significantly influences [Ne II] emission from disks in numerical studies (Schisano et al. 2010). Further factors that have not

been considered in this study include disk gaps and holes (although we showed that our sample of transition disks behaves similar to optically thick disks without jets), grain structure and size distribution, the degree of dust settling, or accretion from the environment onto the disk. Most significantly, unrecognized jets may contribute to some enhancement of [Ne II] emission, as is clearly evident from the subsample with known jets. Most of these additional features require further observational study, and some may remain inaccessible.

7. Conclusions

We have studied [Ne II] emission from a large sample of disk-surrounded pre-main sequence stars, most of them showing optically thick disks (i.e., Class II sources), but some of them additionally ejecting jets, and others showing signatures of transition disks. We have been interested primarily in locating the [Ne II] emission source, but also in finding clues about the ionization and excitation mechanism itself. To this end, we have studied correlations between the observed [Ne II] line luminosity and stellar and circumstellar properties such as the stellar X-ray luminosity, the accretion rate, the mass loss rate, and the luminosity in the [O I] λ6300 line. Our principal findings can be summarized as follows:

– Stars ejecting jets are systematically more luminous in [Ne II], statistically by about one order of magnitude. The difference between jet sources and non-jet sources is in fact so large that the distribution is nearly bi-modal in $L_{\text{[Ne\,II]}}$, with only small overlap between the jet and non-jet sample. The single case of a transition disk with a jet included in this sample (CS Cha) clearly follows the trends for the jet sources, which is expected if the jets produce typically tenfold higher [Ne II] emission than disks.

– A weak correlation is present between $L_{\text{[Ne\,II]}}$ and L_X in the sense that the strongest X-ray sources tend to be strong [Ne II] sources, and the lowest-luminosity [Ne II] sources tend to be X-ray weak, but systematic scatter probably due to unrelated properties in the sources dominates. The correlation is strongest for the jet-driving sources.

– A weak correlation is also present between $L_{\text{[Ne\,II]}}$ and the mass accretion rate, $\dot{M}_{\text{acc}}$. However, such a correlation is not recovered separately for the jet sources and the stars without jets. The best-fit trend between $L_{\text{[Ne\,II]}}$ and $\dot{M}_{\text{acc}}$ is flat for stars without jets. On the other hand, because the jet sources (with their implied high mass loss rates) tend to show both larger accretion rates and higher $L_{\text{[Ne\,II]}}$, an apparent correlation is found that is best explained by the bi-modality of the distributions. We therefore prefer an explanation in which the *mass outflow rate* is the relevant parameter.

– Correlating $L_{\text{[Ne\,II]}}$ with outflow and jet indicators such as EW([O I]), $L_{\text{[O\,I]}}$, or $\dot{M}_{\text{loss}}$, we find several significant correlations, in particular when considering that estimates of $\dot{M}_{\text{loss}}$ are subject to large uncertainties, and equivalent widths relate to the underlying stellar continuum. Note that [O I] emission may also originate in disk surfaces, but trends are also seen separately for the jet-related, high-velocity component of the [O I] line. The trends coherently include jet/outflow sources across a wide range of mass loss parameters and [Ne II] emission.

– Previous theoretical and numerical estimates of [Ne II] fluxes from X-ray/EUV irradiated *disk* surfaces agree with typical [Ne II] fluxes from stars without jets, but they cannot explain the strong [Ne II] emission from a subsample of

putative non-jet objects, and they fail explaining almost all [Ne II] sources from stars with jets. The latter are one to two orders of magnitude more luminous in [Ne II] than predicted by disk models. As shown by Hollenbach & Gorti (2009), shocks in jets easily predict such fluxes. It is well possible that several of the stronger [Ne II] sources also eject hitherto unrecognized jets.

– Considering the absorbing gas column density excesses for CTTS (with respect to WTTS), we suggest that additional gas in accretion streams or disk winds is responsible. This gas will attenuate soft X-rays and EUV photons sufficiently to prevent them from reaching the disk surfaces. If [Ne II] is produced in disks, then the exciting radiation is predominantly X-rays with energies of order 1 keV.

– Transition disks behave, in many ways, like normal optically thick disks without jets. Their [Ne II] luminosity is bounded by 3×10^{28} erg s^{-1}. The similar behavior to optically thick disks probably results from the easy excitation of the [Ne II] transition even in small amounts of gas (Glassgold et al. 2007) at column densities $<10^{21}$ cm^{-2} (Meijerink et al. 2008); the total amount of gas in a disk is therefore of little relevance. Because the transition is excited out to distances of about 25 AU (Meijerink et al. 2008), inner holes in transition disks may also not be of much relevance; on the contrary, reduced winds from the thin inner disk (Hollenbach & Gorti 2009) or less disk gas mass in the way toward larger distances may alleviate excitation of the [Ne II] transition in more extended gas layers.

– The bi-modality of our distributions, with jet sources being substantially more luminous in [Ne II] than non-jet sources, suggests that two different emission mechanisms contribute to [Ne II] emission. There seems to be little doubt that the presence of jets favors strong [Ne II] detections, and the most likely process is [Ne II] emission from the jets themselves, excited either by shocks or also the stellar X-rays at least in the vicinity of the star (Shang et al. 2010). The latter mechanism is supported by a correlation between $L_{[\text{Ne II}]}$ and L_X for jet sources (Fig. 2). On the other hand, non-jet sources fail to follow some trends seen for jet sources; most evidently, $L_{[\text{Ne II}]}$ does not correlate with $\dot{M}_{\text{acc}}$ for these objects, but rather shows a flat distribution in this parameter (Fig. 3, see also Fig. 10).

We conclude that jet ejection leads to enhanced [Ne II] emission, although we cannot demonstrate whether [Ne II] emission forms in shocks close to the star, or in absorbing accretion flows toward the star as the increased mass loss rates of jet engines also implies higher accretion rates, and therefore more massive accretion flows close to the stellar X-ray source.

We still do find indications that the production of [Ne II] emission weakly scales with the X-ray luminosity. This finding supports previous theoretical models of X-ray irradiated and ionized stellar environments although irradiated winds, accretion flows and jets should also be considered as targets, apart from the so far favored disk surface layers. The correlation found between [Ne II] emission from jet-driving CTTS and L_X suggests an important role of stellar short-wavelength radiation in exciting this line in the jet/outflow gas at least relatively close to the stars themselves.

There is obvious need for deeper studies to disentangle the various possible origins of [Ne II] emission. The *Spitzer* beam is large and potentially includes both unresolved outflow and disk contributions. Narrow slit observation using high resolving power, possibly stepped across the source for integral field spectroscopy, could uncover disk line profiles (symmetric, centered at stellar velocity, disk-like velocity range if bound or blue-shifted if photoevaporating) separately from outflow signatures (asymmetric lines, blue-shifted or red-shifted, with high velocities) at larger distances from the star. Such observations have now provided first interesting results (van Boekel et al. 2009; Najita et al. 2009; Pascucci & Sterzik 2009).

References

Acke, B., van den Ancker, M. E., & Dullemond, C. P. 2005, A&A, 436, 209
Aikawa, Y., & Herbst, E. 1999, A&A, 351, 233
Alcalá, J. M., Covino, E., Franchini, M., et al. 1993, A&A, 272, 225
Alcalá, J. M., Spezzi, L., Chapman, N., et al. 2008, ApJ, 676, 427
Alexander, R. D. 2008, MNRAS, 391, L64
Alexander, R. D., Clarke, C. J., & Pringle, J. E. 2004, MNRAS, 354, 71
Alexander, R. D., Clarke, C. J., & Pringle, J. E. 2006, MNRAS, 369, 216
Arnaud, K. A. 1996, in Astronomical Data Analysis Software and Systems V, ed. G. Jacoby, & J. Barnes (San Francisco: ASP), ASP Conf. Ser., 101, 17
Bacciotti, F., & Eislöffel, J. 1999, A&A, 342, 717
Balbus, S. A., & Hawley, J. F. 1991, ApJ, 376, 214
Baldovin-Saavedra, C., Audard, M., Güdel, M., et al. 2010, A&A, submitted
Bally, J., Walawender, J., Luhman, K. L., & Fazio, G. 2006, AJ, 132, 1923
Bary, J. S., Weintraub, D. A., & Kastner, J. H. 2003, ApJ, 586, 1136
Beck, T. L., McGregor, P. J., Takami, M., & Pyo, T.-S. 2008, ApJ, 676, 472
Bergin, E., Calvet, N., Sitko, M. L., et al. 2004, ApJ, 614, L133
Bitner, M. A., Richter, M. J., Lacy, J. H., et al. 2007, ApJ, 661, L69
Blake, G. A., & Boogert, A. C. A. 2004, ApJ, 606, L73
Böhm, K.-H., & Solf, J. 1994, ApJ, 430, 277
Bouwman, J., de Koter, A., Dominik, C., & Waters, L. B. F. M. 2003, A&A, 401, 577
Briceño, C., Luhman, K. L., Hartmann, L., et al. 2002, ApJ, 580, 317
Brittain, S. D., Dimon, T., Najita, J., & Rettig, T. W. 2007, ApJ, 659, 685
Brown, J. M., Blake, G. A., Dullemond, C. P., et al. 2007, ApJ, 664, L107
Calvet, N., D'Alessio, P., Hartmann, L., et al. 2002, ApJ, 568, 1008
Calvet, N., D'Alessio, P., Watson, D. M., et al. 2005, ApJ, 630, L185
Carr, J. S., & Najita, J. R. 2008, Science, 319, 1504
Coffey, D., Bacciotti, F., Ray, T. P., Eislöffel, J., & Woitas, J. 2007, ApJ, 663, 350
Cohen, M., & Kuhi, L. V. 1979, ApJS, 41, 743
Comerón, F., Fernández, M., Baraffe, I., et al. 2003, A&A, 406, 1001
Cox, A. W., Hilton, G. M., Williger, G. M., Grady, C. A., & Woodgate, B. 2005, A&AS, 207, 7419
Dougados, C., Cabrit, S., Lavalley, C., & Ménard, F. 2000, A&A, 357, L61
Duchêne, G., Ghez, A. M., & McCabe, C. 2002, ApJ, 568, 771
Duchêne, G., Ghez, A. M., McCabe, C., & Ceccarelli, C. 2005, ApJ, 628, 832
Dutrey, A., Guilloteau, S., & Guelin, M. 1997, A&A, 317, L55
Ercolano, B., Drake, J. J., Raymond, J. C., & Clarke, C. C. 2008, ApJ, 688, 398
Ercolano, B., Clarke, C. J., & Drake, J. J. 2009, ApJ, 699, 1639
Espaillat, C., Calvet, N., D'Alessio, P., et al. 2007, ApJ, 664, L111
Evans, N. J. II, Allen, L. E., Blake, G. A., et al. 2003, PASP, 115, 810
Favata, F., Micela, G., Silva, B., Sciortino, S., & Tsujimoto, M. 2005, A&A, 433, 1047
Flaccomio, E., Stelzer, B., Sciortino, S., et al. 2009, A&A, 505, 695
Forrest, W. J., Sargent, B., Furlan, E., et al. 2004, ApJS, 154, 443
Gauvin, L. S., & Strom, K. M. 1992, ApJ, 385, 217

Glassgold, A. E., Najita, J., & Igea, J. 2004, ApJ, 615, 972
Glassgold, A. E., Najita, J., & Igea, J. 2007, ApJ, 656, 515
Gómez, M., & Mardones, D. 2003, AJ, 125, 2134
Gorti, U., & Hollenbach, D. 2008, ApJ, 683, 287
Gorti, U., Dullemond, C. P., & Hollenbach, D. 2009, ApJ, 705, 1237
Güdel, M., Briggs, K. R., Arzner, K., et al. 2007a, A&A, 468, 353
Güdel, M., Telleschi, A., Audard, M., et al. 2007b, A&A, 468, 515
Güdel, M., Skinner, S. L., Mel'nikov, S. Y., et al. 2007c, A&A, 468, 529
Güdel, M., Skinner, S. L., Audard, M., et al. 2008, A&A, 478, 797
Güdel, M., van Boekel, R., Lahuis, F., et al. 2009a, in proc. 5th Spitzer Conference, New Light on Young Stars, on-line http://www.ipac.caltech.edu/spitzer2008/talks/ManuelGuedel.html
Güdel, M., Skinner, S. L., Cabrit, S., et al. 2009b, in Protostellar Jets in Context, ed. T. Ray, & K. Tsinganos (Heidelberg: Springer), 347
Hamann, F. 1994, ApJS, 93, 485
Hartigan, P. 1993, AJ, 105, 1511
Hartigan, P., Edwards, S., & Ghandour, L. 1995, ApJ, 452, 736
Hartigan, P., Edwards, S., & Pierson, R. 2004, ApJ, 609, 261
Hartmann, L., Calvet, N., Gullbring, E., & D'Alessio, P. 1998, ApJ, 495, 385
Herczeg, G. J., Linsky, J. L., Valenti, J. A., Johns-Krull, C. M., & Wood, B. E. 2002, ApJ, 572, 310
Herczeg, G. J., Wood, B. E., Linsky, J. L., et al. 2004, ApJ, 607, 369
Herczeg, G. J., Walter, F. M., Linsky, J. L., et al. 2005, AJ, 129, 2777
Herczeg, G. J., Linsky, J. L., Walter, F. M., Gahm, G. F., & Johns-Krull, C. M. 2006, ApJS, 165, 256
Herczeg, G. J., Najita, J. R., Hillenbrand, L. A., & Pascucci, I. 2007, ApJ, 670, 509
Hirth, G. A., Mundt, R., & Solf, J. 1997, A&AS, 126, 437
Hollenbach, D., & Gorti, U. 2009, ApJ, 703, 1203
Hollenbach, D., & McKee, C. F. 1989, ApJ, 342, 306
Houck, J., Roellig, T., van Cleve, J., et al. 2004, ApJS, 154, 18
Hughes, J., Hartigan, P., Krautter, J., et al. 1994, AJ, 108, 1071
Igea, J., & Glassgold, A. E. 1999, ApJ, 581, 848
Ilgner, M., & Nelson, R. P. 2006, A&A, 455, 731
Isobe, T., Feigelson, E. D., & Nelson, P. I. 1986, ApJ, 306, 490
Imanishi, K., Koyama, K., & Tsuboi, Y. 2001, ApJ, 557, 747
Jansen, F., Lumb, D., Altieri, B., et al. 2001, A&A, 365, L1
Jonkheid, B., Faas, F. G. A., van Zadelhoff, G.-J., & van Dishoeck, E. F. 2004, A&A, 428, 511
Kamp, I., & Dullemond, C. P. 2004, ApJ, 615, 991
Kastner, J. H., Franz, G., Grosso, N., et al. 2005, ApJS, 160, 511
Kenyon, S. J., & Hartmann, L. 1995, ApJS, 101, 117
Köhler, R., Ratzka, T., Herbst, T. M., & Kasper, M. 2008, A&A, 482, 929
Krautter, J., Wichmann, R., Schmitt, J. H. M. M., et al. 1997, A&AS, 123, 329
Lada, C. J., Muench, A. A., Luhman, K. L., et al. 2006, AJ, 131, 1574
Lahuis, F., van Dishoeck, E. F., Boogert, A. C. A., et al. 2006, ApJ, 636, L145
Lahuis, F., van Dishoeck, E. F., Blake, G. A., et al. 2007, ApJ, 665, 492
Lavalley, M. P., Isobe, T., & Feigelson, E. D. 1992, in Astronomical Data Analysis Software and Systems I, ed. D. M. Worrall, C. Biemesderfer, & J. Barnes (San Francisco: ASP), 245
Lavalley-Fouquet, C., Cabrit, S., & Dougados, C. 2000, A&A, 356, L41
Luhman, K. L. 2004, ApJ, 602, 816
Meijerink, R., Glassgold, A. E., & Najita, J. R. 2008, ApJ, 676, 518
Meyer, M. R., Hillenbrand, L. A., Backman, D. E., et al. 2004, ApJS, 154, 422
Momose, M., Ohashi, N., Kawabe, R., et al. 1996, ApJ, 470, 1001
Mundt, R., & Eislöffel, J. 1998, AJ, 116, 860
Najita, J., Carr, J. S., & Mathieu, R. D. 2003, ApJ, 589, 931
Najita, J. R., Crockett, N., & Carr, J. S. 2008, ApJ, 687, 1168
Najita, J. R., Doppmann, G. W., Bitner, M. A., Richter, M. J., & Lacy, J. H. 2009, ApJ, 697, 957
Najita, J. R., Strom, S. E., & Muzerolle, J. 2007, MNRAS, 378, 369
Natta, A., Testi, L., & Randich, S. 2006, A&A, 452, 245
Neufeld, D. A., Melnick, G. J., Sonnentrucker, P., et al. 2006, ApJ, 649, 816
Nomura, H., & Millar, T. J. 2005, A&A, 438, 923
Pascucci, I., & Sterzik, M. 2009, ApJ, 702, 724
Pascucci, I., Hollenbach, D., Najita, J., et al. 2007, ApJ, 663, 383
Pontoppidan, K. M., & Dullemond, C. P. 2005, A&A, 435, 595
Pontoppidan, K. M., Blake, G. A., van Dishoeck, E. F., et al. 2008, ApJ, 684, 1323
Ratzka, Th., Leinert, Ch., Henning, Th., et al. 2007, A&A, 471, 173
Rydgren, A. E. 1980, AJ, 85, 438
Salyk, C., Pontoppidan, K. M., Blake, G. A., et al. 2008, ApJ, 676, L49
Salyk, C., Blake, G. A., Boogert, A. C. A., & Brown, J. M. 2009, ApJ, 699, 330
Schisano, E., Ercolano, B., & Güdel, M. 2010, MNRAS, 401, 1336
Seperuelo Duarte, E., Alencar, S. H. P., Batalha, C., et al. 2008, A&A, 489, 349
Shang, H., Glassgold, A. E., Lin, W.-C., & Liu, C.-F. J. 2010, ApJ, 714, 1733
Simon, M., Dutrey, A., & Guilloteau, S. 2000, ApJ, 545, 1034
Skrutskie, M. F., Cutri, R. M., Stiening, R., et al. 2006, AJ, 131, 1163
Solf, J., & Böhm, K. H. 1993, ApJ, 410, L31
Solf, J., & Böhm, K. H. 1999, ApJ, 523, 709
Strüder, L., Briel, U., Dennerl, K., et al. 2001, A&A, 365, L18
Takami, M., Bailey, J., & Chrysostomou, A. 2003, A&A, 397, 675
Telleschi, A., Güdel, M., Briggs, K. R., et al. 2007a, A&A, 468, 541
Telleschi, A., Güdel, M., Briggs, K. R., et al. 2007b, A&A, 468, 425
Tsujimoto, M., Feigelson, E. D., Grosso, N., et al. 2005, ApJS, 160, 503
Turner, M. J. L., Abbey, A., Arnaud, M., et al. 2001, A&A, 365, L27
Valenti, J. A., Johns-Krull, C. M., & Linsky, J. L. 2000, ApJS, 129, 399
van Boekel, R., Waters, L. B. F. M., Dominik, C., et al. 2003, A&A, 400, L21
van Boekel, R., Güdel, M., Henning, Th., Lahuis, F., & Pantin, E. 2009, A&A, 497, 137
van den Ancker, M. E., Wesselius, P. R., Tielens, A. G. G. M., van Dishoeck, E. F., & Spinoglio, L. 199, A&A, 348, 877
Vuong, M. H., Montmerle, T., Grosso, N., et al. 2003, A&A, 408, 581
Webb, R. A., Zuckerman, B., Platais, I., et al. 1999, ApJ, 512, L63
Weintraub, D. A., Kastner, J. H., & Bary, J. S. 2000, ApJ, 541, 767
Weisskopf, M. C., O'Dell, S. L., & vam Speybroeck, L. P. 1996, Proc. SPIE, 2805, 2
Werner, M., Roellig, T., Low, F., et al. 2004, ApJS, 154, 1
White, R. J., & Ghez, A. M. 2001, ApJ, 556, 265
White, R. J., & Hillenbrand, L. A. 2004, ApJ, 616, 998

Table 1. Targets.

Star	Alternative names	RA(J2000.0) (h m s)	Dec(J2000.0) (deg ′ ″)	dist. (pc)
RNO 15	HBC 339, CoKu NGC 1333/2	03 27 47.7	30 12 04.3	250
LkHα 270	HBC 12, NGC 1333 IRS 2	03 29 17.7	31 22 45.1	250
LkHα 271	HBC 13	03 29 21.9	31 15 36.4	250
LkHα 326	HBC 14	03 30 44.0	30 32 46.7	250
LkHα 327	HBC 15, IRAS 03304+3100	03 33 30.4	31 10 50.5	250
LkHα 330	HBC 20, IRAS F03426+3214	03 45 48.3	32 24 11.9	250
IRAS 03446+3254	IRS 4	03 47 47.1	33 04 03.4	250
BP Tau	HBC 32, HD 281934, IRAS 04161+2859	04 19 15.8	29 06 26.9	140
FM Tau	HBC 23, Haro 6-1	04 14 13.6	28 12 49.2	140
T Tau N	HBC 35, HD 284419, IRAS 04190+1924	04 21 59.4	19 32 06.4	140
T Tau S	IRAS 04190+1924	04 21 59.4	19 32 06.4	140
LkCa 8	HBC 385, IP Tau	04 24 57.1	27 11 56.4	140
DG Tau	HBC 37, Ced 33, IRAS 04240+2559	04 27 04.7	26 06 16.3	140
IQ Tau	HBC 41, LkHα 265, IRAS 04267+2600	04 29 51.6	26 06 44.8	140
FX Tau	HBC 44, Haro 6-11, IRAS 04274+2420	04 30 29.6	24 26 45.2	140
DK Tau	HBC 45, IRAS 04276+2554	04 30 44.2	26 01 24.8	140
V710 Tau	HBC 51, LkHα 266, IRAS 04290+1815	04 31 57.8	18 21 36.8	140
GI Tau	HBC 56, Haro 6-21, IRAS 04305+2414	04 33 34.1	24 21 17.0	140
GK Tau	HBC 57, Haro 6-22,	04 33 34.6	24 21 05.9	140
HN Tau	HBC 60, Haro 6-24, St 31, IRAS 04307+1745	04 33 39.4	17 51 52.3	140
DM Tau	HBC 62, IRAS 04309+1803	04 33 48.7	18 10 10.0	140
AA Tau	HBC 63, IRAS 04318+2422	04 34 55.4	24 28 53.2	140
DN Tau	HBC 65, IRAS F04324+2408	04 35 27.4	24 14 58.9	140
CoKu Tau 3	HBC 411	04 35 40.9	24 11 08.5	140
DO Tau	HBC 67, ITG 7	04 38 28.6	26 10 49.9	140
CoKu Tau 4	HBC 421	04 41 16.8	28 40 00.5	140
DP Tau	HBC 70, IRAS 04395+2509	04 42 37.7	25 15 37.5	140
UY Aur	HBC 76, IRAS 04486+3042	04 51 47.4	30 47 13.9	140
GM Aur	HBC 77, IRAS 04519+3017	04 55 11.0	30 21 59.4	140
V836 Tau	HBC 429, IRAS C05000+2519	05 03 06.6	25 23 19.6	140
RW Aur	HBC 80, HD 240764, IRAS 04307+1745	05 07 49.6	30 24 05.2	140
BF Ori	HBC 169, Haro 4-229, IRAS 05348-0636, Par 2510	05 37 13.3	–06 35 00.6	400
IRAS 08267-3336	HBC 562, AT Pyx	08 28 40.7	–33 46 22.4	400
WX Cha	HBC 581, Sz 35, BYB 48, Ced 111 IRS 6, ISO-ChaI 228, IRAS 11085-7720	10 09 58.8	–77 37 08.8	178
SX Cha	HBC 564, Sz 2, BYB 1	10 55 59.7	–77 24 40.0	178
SY Cha	HBC 565, Sz 3, CHX 1, BYB 2, IRAS 10552-7655	10 56 30.5	–77 11 39.5	178
TW Cha	HBC 567, BYB 5, CHXR 5, IRAS 10577-7706	10 59 01.1	–77 22 40.8	178
TW Hya	HBC 568, TWA 1, IRAS 10594-3426	11 01 51.9	–34 42 17.0	57
CS Cha	HBC 569, Sz 9, BYB 10, CHXR 10, IRAS 11011-7717	11 02 25.1	–77 33 36.0	178
BYB 35	ISO-ChaI 101	11 07 21.5	–77 22 11.7	178
CHXR 30	ISO-ChaI 122, ChaI 608	11 08 00.3	–77 17 32.0	178
VW Cha	HBC 575, Sz 24, ISO-ChaI 123, CHXR 31	11 08 01.5	–77 42 28.8	178
VZ Cha	HBC 578, Sz 31, CHXR 39, IRAS 11078-7607, Ced 112 IRS 1	11 09 23.8	–76 23 20.8	178
ISO-ChaI 237	...	11 10 11.4	–76 35 29.0	178
Ced 111 IRS 7	BYB 50, CHXR 47, IRAS 11091-7716	11 10 38.0	–77 32 39.9	178
HM 27	HBC 584, Sz 37, ISO-ChaI 254, IRAS 11093-7701(/10)	11 10 49.6	–77 17 51.7	178
XX Cha	HBC 586, Sz 39, CHXR 49	11 11 39.7	–76 20 15.3	178
RX J1111.7-7620	CHX 18N	11 11 46.3	–76 20 09.2	163
T Cha	HBC 591, IRAS 11547-7904, RX J1157.2-7921	11 57 13.5	–79 21 31.3	66
IRAS 12535-7623	RX J1257.1-7639, SSTc2d J125711.7-764011	12 57 11.8	–76 40 11.6	178
Sz 50	ISO-ChaII 52, SSTc2d J130055.3-771022, RX J1300.9-7710	13 00 55.4	–77 10 22.1	178
ISO-ChaII 54	IRAS F12571-7657, RX J1301.0-7713	13 00 59.2	–77 14 02.8	178
DL Cha	IRAS 13022-7650	13 06 08.4	–77 06 27.4	178
HT Lup	HBC 248, Sz 68, IRAS 15420-3408	15 45 12.9	–34 17 30.5	145
GW Lup	HBC 249, Sz 71, IRAS 15435-3421	15 46 44.7	–34 30 35.5	100
Sz 73	HBC 600	15 47 57.0	–35 14 35.2	100
GQ Lup	HBC 250, Sz 75, IRAS 15459-3529	15 49 12.1	–35 39 04.0	100
IM Lup	HBC 605, Sz 82, IRAS 15528-3747	15 56 09.2	–37 56 05.9	140
RU Lup	HBC 251, Sz 83, HD 142560	15 56 42.3	–37 49 15.6	140
RY Lup	HBC 252, IRAS 15561-4013	15 59 28.4	–40 21 51.1	150
EX Lup	HBC 253, HD 325367, IRAS 15597-4010	16 03 05.5	–40 18 24.8	150
Sz 102	HBC 617, V1190 Sco, HH 228, IRAS 16051-3855, Krautter's Star	16 08 29.7	–39 03 11.2	200

Table 1. Targets (continued).

Star	Alternative names	RA(J2000.0) (h m s)	Dec(J2000.0) (deg ′ ″)	dist. (pc)
AS 205	HBC 254+632, V866 Sco, IRAS 16086-1830	16 11 31.3	–18 38 26.2	120
PZ99 J161411	1RXS J161410.6-230542	16 14 11.1	–23 05 35.8	145
Haro 1-1	HBC 256, V895 Sco	16 21 34.7	–26 12 27.0	125
Haro 1-4	HBC 257, V2503 Oph, DoAr 16, IRAS 16221-2312	16 25 10.5	–23 19 14.5	125
DoAr 24E	HBC 639, ISO-Oph 36, ROX C04	16 26 23.4	–24 21 00.0	125
DoAr 25	ISO-Oph 38, ROXN 1, ROX C03, YLW 34, IRAS 16234-2436	16 26 23.7	–24 43 14.0	125
SR 21	...	16 27 10.3	–24 19 12.4	125
IRS 51	ROXN 66, ISO-Oph 167, IRAS 16246-2436, YLW 45	16 27 39.8	–24 43 15.2	125
SR 9	HBC 264, V2129 Oph, DoAr 34, ISO-Oph 168, ROX 29, IRAS 16246-2415	16 27 40.3	–24 22 04.1	125
V853 Oph	HBC 266, DoAr 40, ROX 34, IRAS 16257-2421	16 28 45.3	–24 28 18.8	125
ROX 42C	IRAS 16282-2427	16 31 15.7	–24 34 01.9	125
ROXs 43A	NTTS 162819-2423S	16 31 20.1	–24 30 05.5	125
IRS 60	IRAS 16284-2418	16 31 30.9	–24 24 39.6	125
Haro 1-16	HBC 268, V2062 Oph, DoAr 44	16 31 33.5	–24 27 37.1	125
Haro 1-17	HBC 648, DoAr 52	16 32 21.9	–24 42 14.9	125
RNO 90	HBC 649, V2132 Oph, V1003 Oph, IRAS 16312-1542	16 34 09.2	–15 48 16.9	140
Wa Oph 6	HBC 653, V2508 Oph, IRAS 16459-1411	16 48 45.6	–14 16 35.8	140
V1121 Oph	HBC 270, AS 209, IRAS 16464-1416	16 49 15.3	–14 22 08.8	125
VV Ser	HBC 282, IRAS 18262+0006	18 28 47.9	00 08 39.8	260
SSTc2d J182900.8[a]	...	18 29 00.9	00 29 31.6	260
SSTc2d J182909.8[b]	...	18 29 09.8	00 34 45.8	260
SSTc2d J182928.2[c]	IRAS 18268-0025	18 29 28.2	–00 22 57.4	260
EC 74	CK 9	18 29 55.7	01 14 31.6	260
EC 82	CK 3	18 29 56.9	01 14 46.7	260
EC 90	CK 1	18 29 57.7	01 14 06.0	260
EC 92	...	18 29 57.9	01 12 51.5	260
CK 4	EC 97	18 29 58.2	01 15 21.6	260
LkHα 348	HBC 285,IRAS 18316-0028	18 34 12.6	–00 26 21.8	260
RX J1842.9-3542	...	18 42 57.9	–35 32 42.7	140
RX J1852.3-3700	IRAS 18489-3703	18 52 17.3	–37 00 12.0	140

Notes. [a] Full name SSTc2d J182900.8+002931. [b] Full name SSTc2d J182909.8+003446. [c] Full name SSTc2d J182928.2+002257 = IRAS 18268-0025 (note error in designation as published in Lahuis et al. 2007; Dec(2000) is <0).

Table 2. Mid-IR and X-ray observations.

Star	Spitzer AOR[a]	X-ray ObsID[b]	X-ray start time[c] y-m-d h:m:s	X-ray stop time[c] y-m-d h:m:s	Total X-ray exposure[c] (s)
RNO 15	5633280	0503670101	2007-07-31 04:55:25	2007-07-31 15:32:31	33135
LkHα 270	5634048	0065820101	2002-02-27 22:48:25	2002-02-28 12:41:45	44808
LkHα 271	11827968	0065820101	2002-02-27 22:48:25	2002-02-28 12:41:45	44808
LkHα 326	5634304	...	...	...	...
LkHα 327	5634560	...	...	...	...
LkHα 330	5634816	...	...	...	...
IRAS 03446+3254	5635072	...	...	...	...
BP Tau	14548224	0200370101	2004-08-15 06:36:51	2004-08-16 18:42:57	116334
FM Tau	15119872	0203542001	2004-09-12 07:21:01	2004-09-12 15:47:38	26760
T Tau N	(VLT)	0301500101	2005-08-15 14:14:33	2005-08-16 12:55:22	65810
T Tau S	(VLT)	0301500101	2005-08-15 14:14:33	2005-08-16 12:55:22	65810
LkCa 8	9832960	...	...	...	...
DG Tau	14547968	0203540201	2004-08-17 06:30:29	2004-08-17 17:27:47	35302
IQ Tau	9832704	0203541401	2005-02-09 03:23:22	2005-02-09 12:25:37	28946
FX Tau	9832448	0203541301	2004-08-25 11:12:21	2004-08-25 20:00:17	(M2) 31251
DK Tau	14548736	0203541401	2005-02-09 03:23:22	2005-02-09 12:25:37	28946
V710 Tau	5636608	0109060301	2000-09-09 19:10:41	2000-09-10 10:18:12	48922
GI Tau	14550528	0203540401	2005-02-21 01:40:40	2005-02-21 10:26:17	27549
GK Tau	14550528	0203540401	2005-02-21 01:40:40	2005-02-21 10:26:17	27549
HN Tau	3532032	0401870201	2007-02-12 17:53:16	2007-02-13 03:20:33	30070
DM Tau	3536384	0554770101	2009-02-10 02:53:12	2009-02-10 13:43:49	34154
AA Tau	14551552	0152680201	2003-02-14 02:40:58	2003-02-14 06:56:35	13719
DN Tau	9831936	0203542101	2005-03-04 20:44:43	2005-03-05 04:56:58	26387
CoKu Tau 3	9831936	0203542101	2005-03-04 20:44:43	2005-03-05 04:56:58	26387
DO Tau	14548480	0501500101	2008-02-22 18:02:57	2008-02-23 01:54:48	24912
CoKu Tau 4	5637888	...	...	...	...
DP Tau	(Gemini N)	0203542201	2005-03-05 06:18:52	2005-03-05 14:39:35	26919
UY Aur	14551040	0401870501	2007-03-19 14:50:12	2007-03-20 01:04:21	31899
GM Aur	18015488	0502100101	2007-09-07 08:53:53	2007-09-07 12:26:11	11048
V836 Tau	3544320	(CXO) 9300	2008-04-07 04:22:00	2008-04-07 06:58:58	8034
RW Aur	3534080	0401870301	2007-02-21 12:10:45	2007-02-21 21:46:22	30538
BF Ori	5638144	0503560601	2007-09-08 08:44:17	2007-09-08 23:45:15	47648
IRAS 08267-3336	5639168	0550120501	2008-06-08 06:26:06	2008-06-08 09:44:43	10507
WX Cha	5640192	0002740501	2002-04-09 10:20:23	2002-04-09 18:59:59	27941
SX Cha	5639424	0152460301	2003-08-18 05:54:03	2003-08-18 14:25:13	(M) 30371
SY Cha	5639424	0067140201	2001-02-24 05:50:17	2001-02-24 15:40:41	32065
TW Cha	5639680	0152460301	2003-08-18 06:15:25	2003-08-18 14:19:20	26301
TW Hya	(Gemini N)	0112880201	2001-07-09 06:35:38	2001-07-09 13:57:31	23957
CS Cha	12695808	0152460301	2003-08-18 06:15:25	2003-08-18 14:19:20	26301
BYB 35	5639680	0203810201	2004-02-27 16:48:11	2004-02-28 00:48:47	(+M12) 26015
CHXR 30	18020096	0203810201	2004-02-27 16:48:11	2004-02-28 00:48:47	26015
VW Cha	5639680	0002740501	2002-04-09 10:20:23	2002-04-09 18:59:59	27941
VZ Cha	5640448	0300270201	2005-09-02 03:33:56	2005-09-03 14:34:33	110399
ISO-ChaI 237	5640448	0203810101	2004-09-28 19:10:05	2004-09-29 02:24:04	23327
Ced 111 IRS 7	5640192	0002740501	2002-04-09 10:20:23	2002-04-09 18:59:59	27941
HM 27	5640192	...	...	...	...
XX Cha	5640448	0300270201	2005-09-02 03:33:56	2005-09-03 14:34:33	110399
RX J1111.7-7620	5451776	0300270201	2005-09-02 03:33:56	2005-09-03 14:34:33	110399
T Cha	5641216	0550120601	2009-03-16 16:51:24	2009-03-16 18:31:58	5282
IRAS 12535-7623	11827456	...	...	...	...
Sz 50	11827456	...	...	...	...
ISO-ChaII 54	15735040	...	...	...	...
DL Cha	5642240	...	...	...	...
HT Lup	5643264[d]	...	...	...	...
GW Lup	5643520	0550120101	2008-08-21 09:04:36	2008-08-21 12:02:22	(+M12) 9122
Sz 73	5644032	...	...	...	...
GQ Lup	5644032	0550120301	2008-08-16 04:30:31	2008-08-16 06:40:27	6862
IM Lup	5644800	0303900401	2005-08-17 09:57:15	2005-08-17 16:52:52	21603
RU Lup	5644800	0303900401	2005-08-17 09:57:15	2005-08-17 16:52:52	21603
RY Lup	5644544	...	...	...	...
EX Lup	5645056	0503590101	2007-08-13 11:51:48	2007-08-13 16:02:18	13245
Sz 102	9407488	0146310201	2003-09-06 06:34:08	2003-09-06 12:23:53	18933

Table 2. Mid-IR and X-ray observations (continued).

Star	*Spitzer* AOR[a]	X-ray ObsID[b]	X-ray start time[c] y-m-d h:m:s	X-ray stop time[c] y-m-d h:m:s	Total X-ray exposure[c] (s)
AS 205	5646080	...	...	...	...
PZ99 J161411	5453824	0109060201	2000-08-24 21:04:08	2000-08-25 11:47:38	47235
Haro 1-1	9833472	...	...	...	...
Haro 1-4	9833216	...	...	...	...
DoAr 24E	5647616	(CXO) 637	2000-05-15 23:35:17	2000-05-17 03:18:30	96443
DoAr 25	12663808	0305540501	2005-03-08 17:52:29	2005-03-09 23:06:18	83963
SR 21	5647616	(CXO) 637	2000-05-15 23:35:17	2000-05-17 03:18:30	96443
IRS 51	9829888	0305540701	2005-03-12 14:36:55	2005-03-12 16:12:36	(M) 56628
SR 9	12027392	...	...	...	...
V853 Oph	12408576	(CXO) 622	2000-07-04 10:13:29	2000-07-04 11:55:10	4812
ROX 42C	6369792	0550120201	2008-08-20 22:39:41	2008-08-21 03:38:34	15773
ROXs 43A	15914496	0550120201	2008-08-20 22:39:41	2008-08-21 03:38:34	15773
IRS 60	6370048	0550120201	2008-08-20 22:39:41	2008-08-21 03:38:34	15773
Haro 1-16	12664064	0550120201	2008-08-20 22:39:41	2008-08-21 03:38:34	15773
Haro 1-17	11827712	0550120201	2008-08-20 22:39:41	2008-08-21 03:38:34	15773
RNO 90	5650432	...	...	...	...
Wa Oph 6	5650688	...	...	...	...
V1121 Oph	5650688	...	...	...	...
VV Ser	5651200	...	...	...	...
SSTc2d J182900.8	13210112	0402820101	2007-04-15 13:52:40	2007-04-16 05:56:38	50802
SSTc2d J182909.8	13210624	0402820101	2007-04-15 13:52:40	2007-04-16 05:56:38	50802
SSTc2d J182928.2	13210368	0550120401	2008-09-19 00:58:20	2008-09-19 08:28:54	23757
EC 74	9407232	0065820201	2003-09-23 03:29:45	2003-09-23 08:29:16	16235
EC 82	9407232	(CXO) 4479	2004-06-19 21:42:42	2004/06/20 23:05:05	88446
EC 90	9828352	0065820201	2003-09-23 03:29:45	2003-09-23 08:29:16	16235
EC 92	9407232	(CXO) 4479	2004-06-19 21:42:42	2004/06/20 23:05:05	88446
CK 4	9407232	(CXO) 4479	2004-06-19 21:42:42	2004/06/20 23:05:05	88446
LkHα 348	9831424	...	...	...	...
RX J1842.9-3542	5451521	...	...	...	...
RX J1852.3-3700	5452033	...	...	...	...

Notes. [a] *Spitzer* AOR = Astronomical Observation Request; for further details on observing setup, see references in Table 3. [b] *XMM-Newton* observation identification number if not otherwise noted; *Chandra* ID if "(CXO)" added. [c] Exposure start and stop times for the *XMM-Newton* EPIC pn camera if not otherwise noted; if (M1), (M2), (M) added, then MOS1, MOS2, or both MOS were used for analysis, and exposure times refer to those detectors; (+M12) indicates that MOS detectors were used additionally to PN for spectral analysis. Exposure times in last column are livetimes for CCD#1 of *XMM-Newton* camera (CCD containing aimpoint of observation for *Chandra*) and are only detector and are only indicative as intervals with high background were selectively and additionally flagged. [d] Also Spitzer AOR 9829120 for HT Lup.

Table 3. Fluxes and luminosities.

Star	$f_{\text{[Ne II]}}$[a] (erg cm^{-2} s^{-1})	$L_{\text{[Ne II]}}$ (erg s^{-1})	$f_{\text{X},0.3-10,\text{abs}}$ (erg cm^{-2} s^{-1})	$L_{\text{X},0.3-10,\text{abs}}$ (erg s^{-1})	$f_{\text{X},0.3-10,\text{unabs}}$ (erg cm^{-2} s^{-1})	$L_{\text{X},0.3-10,\text{unabs}}$ (erg s^{-1})	N_{H}^{b} (10^{22})	Refs.[c]
RNO 15	$<2.6(0.85)\times10^{-14}$	$<1.9\times10^{29}$	3.7×10^{-13}	2.8×10^{30}	1.1×10^{-12}	8.0×10^{30}	4.6	1, X
LkHα 270	$1.3(0.35)\times10^{-14}$	9.7×10^{28}	3.2×10^{-13}	2.4×10^{30}	1.5×10^{-12}	1.1×10^{31}	0.78	1, X
LkHα 271	$<3.6(1.2)\times10^{-15}$	$<2.7\times10^{28}$	3.8×10^{-14}	2.8×10^{29}	1.1×10^{-13}	7.9×10^{29}	3.8	1, X
LkHα 326	$3.1(1.4)\times10^{-15}$	2.3×10^{28}	...	...	...	...	...	1
LkHα 327	$7.8(3.8)\times10^{-15}$	5.8×10^{28}	...	...	...	...	...	1
LkHα 330	$3.8(1.9)\times10^{-15}$	2.8×10^{28}	...	...	...	...	...	1
IRAS 03446+3254	$4.3(0.99)\times10^{-15}$	3.2×10^{28}	...	...	...	...	...	1, X
BP Tau	$2.9(0.4)\times10^{-15}$	6.8×10^{27}	4.3×10^{-13}	1.0×10^{30}	6.1×10^{-13}	1.4×10^{30}	0.09	3, X
FM Tau	$<1.1(0.37)\times10^{-14}$	$<2.6\times10^{28}$	1.5×10^{-13}	3.5×10^{29}	2.2×10^{-13}	5.1×10^{29}	0.15	3, X
T Tau N	$2.0(0.4)\times10^{-13}$	4.7×10^{29}	1.9×10^{-12}	4.4×10^{30}	4.0×10^{-12}	9.4×10^{30}	0.34	5, X
T Tau S	$1.1(0.5)\times10^{-12}$	2.6×10^{30}	...	...	4.0×10^{-12}	9.4×10^{30}	1.6^d	5, X
LkCa 8	$5.0(0.93)\times10^{-15}$	1.2×10^{28}	...	...	...	...	...	1
DG Tau	$2.6(0.09)\times10^{-13}$	6.1×10^{29}	1.3×10^{-13}	3.0×10^{29}	2.3×10^{-13}	5.5×10^{29}	2.1^e	3, X
IQ Tau	$9.9(1.6)\times10^{-15}$	2.3×10^{28}	8.3×10^{-14}	2.0×10^{29}	1.4×10^{-13}	3.2×10^{29}	0.35	1, X
FX Tau	$<5.7(1.9)\times10^{-15}$	$<1.3\times10^{28}$	8.2×10^{-14}	1.9×10^{29}	1.7×10^{-13}	3.9×10^{29}	0.20	1, X
DK Tau	$3.5(0.7)\times10^{-15}$	8.2×10^{27}	2.0×10^{-13}	4.6×10^{29}	3.6×10^{-13}	8.4×10^{29}	0.24	3, X
V710 Tau	$<2.4(0.8)\times10^{-15}$	$<5.6\times10^{27}$	2.5×10^{-13}	5.9×10^{29}	5.0×10^{-13}	1.2×10^{30}	0.23	1, X
GI Tau	$8.4(0.5)\times10^{-15}$	2.0×10^{28}	1.6×10^{-13}	3.8×10^{29}	2.8×10^{-13}	6.7×10^{29}	0.31	3, X
GK Tau	$4.5(0.6)\times10^{-15}$	1.1×10^{28}	2.3×10^{-13}	5.4×10^{29}	5.3×10^{-13}	1.2×10^{30}	0.40	3, X
HN Tau	$2.4(0.48)\times10^{-14}$	5.6×10^{28}	8.0×10^{-14}	1.9×10^{29}	1.4×10^{-13}	3.2×10^{29}	1.1^e	3, X
DM Tau	$5.5(-)\times10^{-15}$	1.3×10^{28}	5.7×10^{-13}	1.3×10^{30}	8.4×10^{-13}	2.0×10^{30}	0.14	6, X
AA Tau	$1.2(0.04)\times10^{-14}$	2.8×10^{28}	2.0×10^{-13}	4.6×10^{29}	4.4×10^{-13}	1.0×10^{30}	0.93	3, X
DN Tau	$<4.2(1.4)\times10^{-15}$	$<9.9\times10^{27}$	3.7×10^{-13}	8.7×10^{29}	4.6×10^{-13}	1.1×10^{30}	0.058	1, X
CoKu Tau 3	$3.8(1.5)\times10^{-15}$	8.9×10^{27}	1.1×10^{-12}	2.6×10^{30}	2.4×10^{-12}	5.7×10^{30}	0.38	1, X
DO Tau	$8.0(0.9)\times10^{-15}$	1.9×10^{28}	3.1×10^{-14}	7.3×10^{28}	1.0×10^{-13}	2.4×10^{29}	0.63	3, X
CoKu Tau 4	$2.7(0.8)\times10^{-15}$	6.3×10^{27}	...	...	...	...	...	1
DP Tau	$<1.1(0.55)\times10^{-14}$	$<2.6\times10^{28}$	1.8×10^{-14}	4.2×10^{28}	4.2×10^{-14}	9.9×10^{28}	3.8^e	4, X
UY Aur	$2.2(0.28)\times10^{-14}$	5.2×10^{28}	1.1×10^{-13}	2.6×10^{29}	1.7×10^{-13}	4.0×10^{29}	0.12	3, X
GM Aur	$1.2(0.06)\times10^{-14}$	2.8×10^{28}	5.1×10^{-13}	1.2×10^{30}	6.8×10^{-13}	1.6×10^{30}	0.11	3, X
V836 Tau	$1.1(0.65)\times10^{-14}$	2.6×10^{28}	4.6×10^{-13}	1.1×10^{30}	7.2×10^{-13}	1.7×10^{30}	0.23	3, C
RW Aur	$<8.2(2.0)\times10^{-15}$	$<1.9\times10^{28}$	4.0×10^{-13}	9.4×10^{29}	7.0×10^{-13}	1.6×10^{30}	0.22	3, X
BF Ori	$<1.4(0.48)\times10^{-14}$	$<2.7\times10^{29}$	1.4×10^{-14}	2.7×10^{29}	1.7×10^{-13}	3.2×10^{30}	0.04	1, X
IRAS 08267-3336	$8.3(1.2)\times10^{-15}$	1.6×10^{29}	4.9×10^{-14}	9.3×10^{29}	9.3×10^{-13}	1.8×10^{31}	0.86	1, X
WX Cha	$<4.8(1.6)\times10^{-15}$	$<1.8\times10^{28}$	2.8×10^{-13}	1.1×10^{30}	1.2×10^{-12}	4.6×10^{30}	0.58	1, X
SX Cha	$<8.1(2.7)\times10^{-15}$	$<3.1\times10^{28}$	4.5×10^{-14}	1.7×10^{29}	6.7×10^{-14}	2.6×10^{29}	0.15	1, X
SY Cha	$2.6(1.0)\times10^{-15}$	9.9×10^{27}	1.3×10^{-13}	4.8×10^{29}	1.8×10^{-13}	6.9×10^{29}	0.10	1, X
TW Cha	$<3.3(1.1)\times10^{-15}$	$<1.3\times10^{28}$	2.0×10^{-13}	7.5×10^{29}	3.7×10^{-13}	1.4×10^{30}	0.18	1, X
TW Hya	$5.9(1.1)\times10^{-14}$	2.3×10^{28}	4.0×10^{-12}	1.5×10^{30}	5.3×10^{-12}	2.1×10^{30}	0.044	4, X
CS Cha	$4.3(-)\times10^{-14}$	1.6×10^{29}	8.2×10^{-13}	3.1×10^{30}	1.0×10^{-12}	3.8×10^{30}	0.042	6, X
BYB 35	$<1.2(0.4)\times10^{-15}$	$<4.6\times10^{27}$	...	...	$<1.1\times10^{-13}$	$<4.3\times10^{29}$	3.8^f	1, X
CHXR 30	$<2.1(0.7)\times10^{-15}$	$<8.0\times10^{27}$	1.4×10^{-13}	5.2×10^{29}	9.8×10^{-13}	3.7×10^{30}	1.2	3, X
VW Cha	$3.7(0.33)\times10^{-14}$	1.4×10^{29}	6.4×10^{-13}	2.4×10^{30}	2.2×10^{-12}	8.3×10^{30}	0.48	1, X
VZ Cha	$3.8(1.70)\times10^{-15}$	1.4×10^{28}	6.6×10^{-14}	2.5×10^{29}	1.4×10^{-13}	5.3×10^{29}	0.21	1, X
ISO-ChaI 237	$<6.0(2.0)\times10^{-15}$	$<2.3\times10^{28}$	3.7×10^{-14}	1.4×10^{29}	2.5×10^{-13}	9.4×10^{29}	1.1	1, X
Ced 111 IRS 7	$<1.8(0.6)\times10^{-15}$	$<6.8\times10^{27}$	1.4×10^{-13}	5.3×10^{29}	2.7×10^{-13}	1.0×10^{30}	0.45	1, X
HM 27	$<3.0(1.0)\times10^{-15}$	$<1.1\times10^{28}$	...	...	...	...	...	1
XX Cha	$5.0(1.1)\times10^{-15}$	1.9×10^{28}	1.3×10^{-13}	4.8×10^{29}	2.8×10^{-13}	1.1×10^{30}	0.34	1, X
RX J1111.7-7620	$5.1(1.2)\times10^{-15}$	1.6×10^{28}	4.6×10^{-13}	1.5×10^{30}	8.7×10^{-13}	2.8×10^{30}	0.25	2, X
T Cha	$3.2(0.10)\times10^{-14}$	1.7×10^{28}	5.1×10^{-13}	2.7×10^{29}	2.0×10^{-12}	1.1×10^{30}	0.97	1, X
IRAS 12535-7623	$<3.9(1.3)\times10^{-15}$	$<1.5\times10^{28}$	...	...	...	...	...	1
Sz 50	$2.8(0.77)\times10^{-16}$	1.1×10^{27}	...	...	...	...	...	1
ISO-ChaII 54	$5.6(0.91)\times10^{-15}$	2.1×10^{28}	...	...	...	...	...	1
DL Cha	$<6.3(2.1)\times10^{-13}$	$<2.4\times10^{30}$	...	...	...	...	...	1
HT Lup	$<2.9(0.96)\times10^{-14}$	$<7.3\times10^{28}$	...	...	...	...	...	1
GW Lup	$<2.1(0.7)\times10^{-15}$	$<2.5\times10^{27}$	1.8×10^{-13}	2.1×10^{29}	2.4×10^{-13}	2.9×10^{29}	0.098	1, X
Sz 73	$2.1(0.26)\times10^{-14}$	2.5×10^{28}	...	...	...	...	...	1
GQ Lup	$<8.1(2.7)\times10^{-15}$	$<9.7\times10^{27}$	3.3×10^{-13}	3.9×10^{29}	6.2×10^{-13}	7.4×10^{29}	0.47	1, X
IM Lup	$9.8(1.5)\times10^{-15}$	2.3×10^{28}	9.9×10^{-13}	2.3×10^{30}	1.4×10^{-12}	3.2×10^{30}	0.11	1, X
RU Lup	$2.6(0.83)\times10^{-14}$	6.1×10^{28}	2.7×10^{-13}	6.4×10^{29}	4.3×10^{-13}	1.0×10^{30}	0.14	1, X
RY Lup	$<9.6(3.2)\times10^{-15}$	$<2.6\times10^{28}$	...	...	...	...	...	1
EX Lup	$<6.6(2.2)\times10^{-15}$	$<1.8\times10^{28}$	4.7×10^{-13}	1.3×10^{30}	5.5×10^{-13}	1.5×10^{30}	0.033	1, X
Sz 102	$3.6(0.15)\times10^{-14}$	1.7×10^{29}	8.6×10^{-15}	4.1×10^{28}	3.8×10^{-14}	1.8×10^{29}	0.24	1, X

Table 3. Fluxes and luminosities (continued).

Star	$f^a_{[\mathrm{Ne\,II}]}$ (erg cm^{-2} s^{-1})	$L_{[\mathrm{Ne\,II}]}$ (erg s^{-1})	$f_{\mathrm{X,0.3-10,abs}}$ (erg cm^{-2} s^{-1})	$L_{\mathrm{X,0.3-10,abs}}$ (erg s^{-1})	$f_{\mathrm{X,0.3-10,unabs}}$ (erg cm^{-2} s^{-1})	$L_{\mathrm{X,0.3-10,unabs}}$ (erg s^{-1})	N^b_{H} (10^{22})	Refs.^{c}
AS 205	$< 8.1(2.7) \times 10^{-14}$	$<1.4 \times 10^{29}$	...	...	...	...	...	1
PZ99 J161411	$6.2(1.8) \times 10^{-15}$	1.6×10^{28}	1.7×10^{-12}	4.2×10^{30}	2.5×10^{-12}	6.2×10^{30}	0.12	2, X
Haro 1-1	$3.2(0.91) \times 10^{-15}$	6.0×10^{27}	...	...	...	...	...	1
Haro 1-4	$1.1(0.16) \times 10^{-14}$	2.1×10^{28}	...	...	...	...	...	1
DoAr 24E	$<3.6(1.2) \times 10^{-14}$	$<6.7 \times 10^{28}$	1.0×10^{-13}	1.9×10^{29}	3.0×10^{-13}	5.6×10^{29}	1.2	1, C
DoAr 25	$2.8(0.5) \times 10^{-15}$	5.2×10^{27}	2.3×10^{-13}	4.3×10^{29}	1.5×10^{-12}	2.8×10^{30}	1.5	3, X
SR 21	$< 3.0(1.0) \times 10^{-14}$	$<5.6 \times 10^{28}$	6.9×10^{-14}	1.3×10^{29}	5.5×10^{-13}	1.0×10^{30}	1.1	1, C
IRS 51	$7.9(2.8) \times 10^{-15}$	1.5×10^{28}	2.3×10^{-13}	4.3×10^{29}	1.8×10^{-12}	3.4×10^{30}	3.7	1, X
SR 9	$7.2(1.9) \times 10^{-15}$	1.3×10^{28}	...	...	...	...	...	1, X
V853 Oph	$1.6(0.16) \times 10^{-14}$	3.0×10^{28}	7.7×10^{-13}	1.4×10^{30}	1.7×10^{-12}	3.1×10^{30}	0.26	1, C
ROX 42C	$5.0(1.2) \times 10^{-15}$	9.4×10^{27}	1.1×10^{-12}	2.1×10^{30}	2.4×10^{-12}	4.5×10^{30}	0.39	1, X
ROXs 43A	$<2.2(0.73) \times 10^{-14}$	$<4.1 \times 10^{28}$	2.2×10^{-12}	4.2×10^{30}	5.0×10^{-12}	9.4×10^{30}	0.39	1, X
IRS 60	$1.4(0.42) \times 10^{-14}$	2.6×10^{28}	8.5×10^{-14}	1.6×10^{29}	1.4×10^{-13}	2.6×10^{29}	0.41	1, X
Haro 1-16	$6.8(3.3) \times 10^{-15}$	1.3×10^{28}	2.9×10^{-13}	5.3×10^{29}	6.8×10^{-13}	1.3×10^{30}	0.35	1, X
Haro 1-17	$1.6(0.4) \times 10^{-15}$	3.0×10^{27}	1.6×10^{-13}	3.0×10^{29}	3.1×10^{-13}	5.8×10^{29}	0.25	1, X
RNO 90	$2.4(0.84) \times 10^{-14}$	5.6×10^{28}	...	...	...	...	...	1
Wa Oph 6	$9.1(3.8) \times 10^{-15}$	2.1×10^{28}	...	...	...	...	...	1
V1121 Oph	$1.9(0.69) \times 10^{-14}$	3.6×10^{28}	...	...	...	...	...	1
VV Ser	$<3.9(1.3) \times 10^{-14}$	$<3.2 \times 10^{29}$	...	...	...	...	...	1
SSTc2d J182900.8	$<4.8(1.6) \times 10^{-15}$	$<3.9 \times 10^{28}$	3.6×10^{-14}	2.9×10^{29}	7.0×10^{-14}	5.7×10^{29}	0.51	1, X
SSTc2d J182909.8	$<1.3(0.44) \times 10^{-14}$	$<1.1 \times 10^{29}$	(undet)	(undet)	(undet)	(undet)	...	1, X
SSTc2d J182928.2	$1.0(0.11) \times 10^{-13}$	8.1×10^{29}	(undet)	(undet)	(undet)	(undet)	...	1, X
EC 74	$4.2(1.1) \times 10^{-15}$	3.4×10^{28}	2.8×10^{-13}	2.2×10^{30}	5.4×10^{-13}	4.3×10^{30}	2.1	1, X
EC 82	$7.1(2.6) \times 10^{-15}$	5.8×10^{28}	2.4×10^{-15}	1.9×10^{28}	1.1×10^{-14}	9.2×10^{28}	1.1	1, C
EC 90	$<6.0(2.0) \times 10^{-14}$	$<4.9 \times 10^{29}$	2.6×10^{-13}	2.1×10^{30}	9.3×10^{-13}	7.6×10^{30}	1.9	1, X
EC 92	$1.5(0.12) \times 10^{-14}$	1.2×10^{29}	1.7×10^{-13}	1.4×10^{30}	1.2×10^{-12}	9.5×10^{30}	5.6	1, C
CK 4	$<3.6(1.2) \times 10^{-15}$	$<2.9 \times 10^{28}$	1.2×10^{-14}	9.6×10^{28}	8.8×10^{-14}	7.2×10^{29}	1.4	1, C
LkHα 348	$<6.6(2.2) \times 10^{-14}$	$<5.4 \times 10^{29}$	...	...	...	...	...	1
RX J1842.9-3542	$4.3(1.3) \times 10^{-15}$	1.0×10^{28}	...	...	...	...	...	2
RX J1852.3-3700	$7.2(0.4) \times 10^{-15}$	1.7×10^{28}	...	...	...	...	...	2

Notes. $^{(a)}$ Errors are given in parentheses. $^{(b)}$ In units of 10^{22} cm^{-2}. $^{(c)}$ References: 1: New analysis of Spitzer c2d sample, for original analysis see Lahuis et al. (2007); 2: Pascucci et al. (2007); 3: archival GTO/GO observations, see Najita & Carr (in prep.); 4: Herczeg et al. (2007); 5: van Boekel et al. (2009); 6: Espaillat et al. (2007); C: from *Chandra* archive; X: from *XMM-Newton* archive. $^{(d)}$ Same intrinsic (unabsorbed) L_X as for T Tau N assumed (similar stellar masses). Minimum N_H based on minimum estimated visual extinction of 8 mag (Duchêne et al. 2005). $^{(e)}$ N_H and f_X only for hard (coronal) component in Two Absorber X-ray spectra (Güdel et al. 2007b, 2009b). $^{(f)}$ N_H adopted based on published A_V or A_J (see text for details).

Table 4. Additional parameters.

Star	$\log \dot{M}_{\rm acc}$ ($M_\odot$ yr^{-1})	$EW({\rm H}\alpha)$ (Å)	$EW({\rm [O\,I]}_f)$ (Å)	$EW({\rm [O\,I]}_t)$ (Å)	$\log L_{\rm [OI],f}$ ($L_\odot$)	$\log L_{\rm [OI],t}$ ($L_\odot$)	$\log \dot{M}_{\rm loss}$ ($M_\odot$ yr^{-1})	jet? TD?[a]	Refs.[b]
RNO 15	...	...	...	...	...	...	...	...	...
LkHα 270	...	30.9	...	...	...	...	...	...	6
LkHα 271	...	185.7	...	...	...	...	...	...	6
LkHα 326	...	52.7	...	0.8	...	...	...	...	6
LkHα 327	...	51.0	...	0.9	...	...	...	...	6
LkHα 330	...	20.3	...	...	...	...	...	T	6, 31
IRAS 03446+3254	...	...	...	...	...	...	...	...	...
BP Tau	−7.54	40–92	0.07	0.26	−5.71	−4.75	<−9.7	...	13, X, 12
FM Tau	−8.45	62–71	0.045	0.48	−6.37	−5.19	<−10.6	...	21, 35, 6, 12
T Tau N	−7.12	38–60	...	2.0	...	−2.78	−6.96	J	21, 6, 26, 4, (27)
T Tau S	...	...	...	...	...	...	...	J	4
LkCa 8	−9.10	...	0.24	0.63	−5.3	−4.77	−9.6	...	13, 12
DG Tau	−6.30	63–125	12.4	17.5	−2.21	−2.07	−6.5	J	21, X, 12, 29
IQ Tau	−7.55	8–17	...	0.4	...	−4.89	...	...	21, 6, (5, 27)
FX Tau	−8.65	9.6	...	...	...	...	...	...	21, 6
DK Tau	−7.42	19–50	0.36	0.79	−4.23	−3.90	−8.5	...	13, X, 12
V710 Tau	...	34–89	...	0.3	...	−5.00	...	...	X, 6, (5, 27)
GI Tau	−8.02	15–21	0.11	0.48	−5.11	−4.46	−9.4	...	13, X, 12
GK Tau	−8.19	15–35	0.20	0.51	−4.88	−4.48	−9.2	...	13, X, 12
HN Tau	−8.60	120–163	5.7	13.2	−3.82	−3.46	−8.1	J	35, 6, 12, 37
DM Tau	−7.95	139	...	...	...	...	...	T	13, 6, 33
AA Tau	−8.48	37–46	0.16	1.25	−4.77	−3.88	−9.1	J	13, X, 12, 30
DN Tau	−8.46	12–87	0.1	0.53	−5.07	−4.34	−9.4	...	21, X, 12
CoKu Tau 3	...	5	...	...	...	...	...	...	6
DO Tau	−6.84	100–109	2.63	3.60	−3.20	−3.06	−7.5	J	13, X, 12, 17
CoKu Tau 4	<−10.0	...	...	...	...	...	...	T	21, 34
DP Tau	−7.88	74–102	0.7	0.7	−4.78	−4.78	−7.42	J	13, X, 17, 26, 28, (27)
UY Aur	−7.18	36–73	1.15	2.30	−3.91	−3.62	−8.2	J	13, X, 12, 17
GM Aur	−8.02	96–97	0.015	0.27	−6.25	−4.90	<−10.0	T	13, X, 12, 33
V836 Tau	−7.86	25	0.02	0.35	−6.60	−4.94	<−10.1	T	26, 12, 38
RW Aur	−7.12	42-84	1.18	1.59	−3.26	−3.11	−7.6	J	21, 6, 26, 35, 12, 36
BF Ori	...	6.4	...	...	...	...	...	...	6
IRAS 08267-3336	...	...	...	...	...	...	...	...	...
WX Cha	−8.47	66	...	...	...	...	...	...	11, 9
SX Cha	−8.37	27	...	...	...	...	...	...	13, 9
SY Cha	−8.60	8–64	...	...	...	...	...	...	13, 20&9
TW Cha	...	26–41	...	0.95	...	−3.84	...	...	20&9, 10, (9)
TW Hya	−8.70	220	...	0.67	...	−5.06	...	T	14, 40, 16, 32
CS Cha	−7.92	13–65	...	...	...	...	...	J, T	8, 9&11, 25, 8
BYB 35	...	...	...	...	...	...	...	...	...
CHXR 30	...	1	...	...	...	...	...	...	20
VW Cha	−6.95	71–147	...	0.93	...	−3.63	...	J	13, 20&9, 10, 3, (9)
VZ Cha	−8.28	71.4	...	0.42	...	−4.75	...	...	13, 9, 10, (9)
ISO-ChaI 237	...	3.8	...	...	...	...	...	..	20
Ced 111 IRS 7	...	...	...	...	...	...	...	...	...
HM 27	...	102–201	...	...	...	...	...	...	20&9
XX Cha	−9.07	90–134	...	...	...	...	...	...	13, 20&9
RX J1111.7-7620	−9.30	7.7	...	...	...	...	...	T	22, 20
T Cha	...	2-7	...	...	...	...	...	T	41, 31
IRAS 12535-7623	...	...	...	...	...	...	...	...	...
Sz 50	...	...	...	...	...	...	...	J	1
ISO-ChaII 54	...	...	...	...	...	...	...	...	...
DL Cha	...	...	...	...	...	...	...	...	...
HT Lup	...	2.8	...	<0.03	...	<−5.02	...	...	18, 10, (M, 19)
GW Lup	...	90.3	...	...	...	...	...	...	18
Sz 73	...	97.2	...	...	...	...	...	...	18
GQ Lup	−7.50	38.6	...	0.08	...	−5.34	...	...	24, 18, 10, (M, 19)
IM Lup	...	8.1	...	...	...	...	...	...	18
RU Lup	−7.30	216.4	0.79	1.94	−4.3	−3.95	...	J	15, 18, 10, 25, (S, M, 15)
RY Lup	...	...	...	...	...	...	...	...	...
EX Lup	...	...	...	...	...	...	...	...	...
Sz 102	−8.10	377.4	...	...	...	...	...	J	7, 18, 2

Table 4. Additional parameters (continued).

Star	$\log \dot{M}_{\rm acc}$ ($M_\odot$ yr^{-1})	EW(Hα) (Å)	EW([O I]$_f$) (Å)	EW([O I]$_t$) (Å)	$\log L_{\rm [OI],f}$ ($L_\odot$)	$\log L_{\rm [OI],t}$ ($L_\odot$)	$\log \dot{M}_{\rm loss}$ ($M_\odot$ yr^{-1})	jet? TD?[a]	Refs.[b]
AS 205	...	154.6	...	1.8	...	3.16	...	...	6, (M, 6)
PZ99 J161411	−9.50	...	...	...	...	...	...	T	22
Haro 1-1	...	123	...	0.52	...	−4.62	...	...	6,10,(S,6)
Haro 1-4	...	47.6	...	...	...	...	...	...	6
DoAr 24E	−8.21	...	...	...	...	...	...	...	39
DoAr 25	<−9.24	...	...	...	...	...	...	...	39
SR 21	<−8.84	...	...	...	...	...	...	T	39, 31
IRS 51	...	...	...	...	...	...	...	...	...
SR 9	−8.26	11.6	...	0.06	...	−6.00	...	...	39, 6, 10, (S, 6)
V853 Oph	−8.31	42	...	...	...	...	...	...	39, 23
ROX 42C	...	...	...	...	...	...	...	...	...
ROXs 43A	...	...	...	...	...	...	...	...	...
IRS 60	...	...	...	...	...	...	...	...	...
Haro 1-16	...	59	...	...	...	...	...	...	6
Haro 1-17	...	15	...	...	...	...	...	...	23
RNO 90	...	...	...	...	...	...	...	...	...
Wa Oph 6	...	...	...	...	...	...	...	...	...
V1121 Oph	...	...	...	...	...	...	...	...	...
VV Ser	...	...	..	...	...	...	...	...	...
SSTc2d J182900.8	...	...	...	...	...	...	...	...	...
SSTc2d J182909.8	...	...	...	...	...	...	...	...	...
SSTc2d J182928.2	...	...	...	...	...	...	...	...	...
EC 74	...	...	...	...	...	...	...	...	...
EC 82	...	...	...	...	...	...	...	...	...
EC 90	...	...	...	...	...	...	...	...	...
EC 92	...	...	...	...	...	...	...	...	...
CK 4	...	...	...	...	...	..	...	...	...
LkHα 348	...	310	...	0.6	...	..	...	...	6
RX J1842.9-3542	−9.0	...	...	...	...	..	...	T	22
RX J1852.3-3700	−9.3	...	...	...	...	..	...	T	22

Notes. [a] T = transitional disk (either "anemic" or "cold" disk); J = jet-driving object. [b] References: 1 Alcalá et al. (2008); 2 Bacciotti & Eislöffel (1999); 3 Bally et al. (2006); 4 Böhm & Solf (1994); 5 Briceño et al. (2002); 6 Cohen & Kuhi (1979); 7 Comerón et al. (2003); 8 Espaillat et al. (2007); 9 Gauvin & Strom (1992); 10 Hamann (1994); 11 Hartigan (1993); 12 Hartigan et al. (1995); 13 Hartmann et al. (1998); 14 Herczeg et al. (2004); 15 Herczeg et al. (2005); 16 Herczeg et al. (2007); 17 Hirth et al. (1997); 18 Hughes et al. (1994); 19 Krautter et al. (1997); 20 Luhman (2004); 21 Najita et al. (2007); 22 Pascucci et al. (2007); 23 Rydgren (1980); 24 Seperuelo Duarte et al. (2008); 25 Takami et al. (2003); 26 White & Hillenbrand (2004); 27 Kenyon & Hartmann (1995); 28 Mundt & Eislöffel (1998); 29 Solf & Böhm (1993); 30 Cox et al. (2005); 31 Brown et al. (2007); 32 Calvet et al. (2002); 33 Calvet et al. (2005); 34 Forrest et al. (2004); 35 White & Ghez (2001); 36 Dougados et al. (2000); 37 Hartigan et al. (2004); 38 Najita et al. (2008); 39 Natta et al. (2006); 40 Webb et al. (1999); 41 Alcalá et al. (1993). M: 2MASS; S: SIMBAD; X: XEST survey, see Güdel et al. (2007a) and references therein. References in parentheses are for complementary data, e.g., $A_{\rm V}$ or R magnitude, used to calculate $\log L_{\rm [OI]}$.